CMOS 5^{th} DERIVATIVE GAUSSIAN IMPULSE GENERATOR FOR UWB APPLICATION

by

SHIN-CHIH CHANG

Presented to the Faculty of the Graduate School of

The University of Texas at Arlington in Partial Fulfillment

of the Requirements

for the Degree of

MASTER OF SCIENCE ELECTRICAL ENGINEERING

THE UNIVERSITY OF TEXAS AT ARLINGTON

December 2005

ACKNOWLEDGEMENTS

I like to thank my adviser Dr. Sungyong Jung for agreeing to supervise me on this topic and giving me lots of priceless guidance. I sincerely thank for his ideas, encouragement and insights throughout the course of this thesis. Without his invaluable support, I can not make the completion of this work. I thank Dr. Jean Gao and Dr. Jonathan Bredow for agreeing to be a part of my thesis committee and giving me very valuable guidance.

I would also like to thank all AMIC members for providing good environment for this work. Special thanks to Tim Merkin, Youngjune Kim, and David Maxwell for their timely help.

I am very grateful to my parents. During this period of time, they offer the most important things to me. I would like to mention my lovely kid, Timothy. When I was working day and night, you are always in my heart. Hope one day you grow up, you can understand what I am considering about right now. I also thank my husband for supporting me in the school. Thanks to all my friends who have been with me to provide moral support to complete this work successfully. This thesis is dedicated to them.

November 8, 2005

ABSTRACT

CMOS 5th DERIVATIVE GAUSSIAN IMPULSE GENERATOR FOR UWB APPLICATION

Publication No. ______

Shin-Chih Chang, M.S.

The University of Texas at Arlington, 2005

Supervising Professor: Dr. Sungyong Jung

Ultra-Wide Bandwidth radio has become a very promising Wireless technology. It possesses major attractive advantages in Wireless Communications, networking, radar, imaging, and positioning systems. UWB impulse radio signals provide an extremely broad bandwidth for transmission and very high data rate over short distance. An all CMOS impulse generator implemented in an Ultra-Wide-Bandwidth (UWB) wireless communication system was designed. The designed impulse generator as the initial and important component in UWB wireless communication generates a 5th derivative Gaussian pulse for transmission. The impulse generator consists of four interpolation delay blocks, an XOR block, and an FIR filter. The interpolation delay blocks uses voltage to adjust the delay time by controlling the gains of each path. By

adjusting the delay time, impulse generator can achieve the required frequency. The XOR gate is implemented using a Gilbert cell. When the two different input signals have two opposite levels at the same time, the XOR gate creates a pulse. After the XOR gate, a Gaussian pulse is generated and then it goes through the FIR filter. An FIR filter is used as the band pass filter, with 15 delay-taps, it shapes the Gaussian pulse. The FIR filter is designed and simulated using Matlab. The function firpm using the Parks-McClellan algorithm was used to optimize the impulse response of the FIR filter. The FIR filter as the pulse shaper convolves with the input signal – a Gaussian pulse to generate the 5^{th} derivative Gaussian pulse. After pulse shaping with the FIR filter, the 5^{th} derivative Gaussian pulse is generated to meet the FCC transmit mask. The 5^{th} derivative Gaussian pulse provides the maximum bandwidth and also it meets the power spectrum density spec of FCC regulations. The design and simulation of the impulse generator was performed using the Advanced Design System (ADS) in a TSMC 0.18μm CMOS process. The FIR filter was designed and simulated in MATLAB. The whole circuit's simulation uses ADS and MATLAB co-simulation.

TABLE OF CONTENTS

LIST OF ILLUSTRATIONS

LIST OF TABLES

CHAPTER 1

INTRODUCTION

Recently, UWB wireless technology has been attractive to replace narrowband wireless technologies. UWB radios operate using low-power ultra-short information bearing pulses. UWB characterizes transmission systems with spectral occupancy over 500 MHz or a fractional bandwidth of more than 20%. This huge bandwidth provides an excellent opportunity for an enormous number of bandwidth-demanding position-critical lower-power applications in wireless communications, networking, radar imaging, and localization system. Such systems depend on ultra-short waveforms and can be free of carriers [1].

One of the technologies of UWB is called impulse radio (IR). Impulse radio, modulating data in the time domain, improves data throughput with low power consumption. Impulse radio does not use a sinusoidal carrier to shift the signal to a higher frequency, but instead communicates with a baseband signal composed of subnano second pulses. Impulse radio systems employ a pulse train with pulse amplitude modulation (PAM) or pulse-position modulation (PPM) also biphase modulation [4]. It transmits ultra-short duration pulses to make the spectrum of the UWB signal several gigahertz wide. Because of the short duration with a wide fractional channel bandwidth of the pulse, it leads to lower worst- case multipath fading and provides an excellent immunity to interference from other radio systems even in propagation environments. Implementing impulse radio UWB transceivers with mostly digital circuits using no intermediate frequency (IF) processing makes it easier and cheaper compared with the typical spread spectrum transceivers – as used in Bluetooth and WiFi. Those typical characteristics mark impulse radio as the best candidate for UWB systems [3].

In UWB systems, an impulse generator is one of the key components to enable IR UWB communications. In addition, selecting the fundamental pulse shape used to generate the IR UWB signal is one of the important considerations [2]. The signal should produce the best transmission capacity and low interrupt characteristics to perform the ultimate information transmission rate and long operation range.

Gaussian pulses present an excellent time-frequency resolution result, typically in their differentiations. The first derivative Gaussian pulse is easily generated. However, the PSD of the first derivative pulse does not meet the FCC emission requirements. For wireless communications in particular, the FCC regulated power levels in the band from 3.1 GHz to 10.6 GHz are very low (below -41.3 dBm). For meeting the FCC mask, one approach is modulating the monocycle pulse with a sinusoid, but it will increase the cost and complexity. The other approach is to take derivatives of the pulse. The higher orders of the derivative of the pulse, the more zero crossings in the same pulse width corresponding to a higher "carrier" frequency sinusoid modulated by an equivalent Gaussian envelop. These observations make us to consider high-order derivatives of the Gaussian pulse for UWB transmission. For indoor UWB systems, considering the order of derivative and bandwidth, a fifth-order derivative pulse is the selected candidate [2] [4]. Thus, we will focus on designing an impulse generator which fits the power spectrum density (PSD) of the FCC mask in this paper.

The UWB transmitter generates and transmits very short duration pulses as signals without a carrier. The functional block diagram of the UWB transmitter (Tx) is shown in Fig.1. The proposed impulse generator consists of a pulse generator and an FIR filter. Examining some previously designed UWB pulse generators [12], [13], [2], reveals that their generated pulses are not the 5^{th} derivative Gaussian pulse, including the other all-CMOS impulse generators [11]. Implementing the designed FIR filter on the Gaussian pulse from the pulse generator can form the exact fifth-order derivative Gaussian pulse. The fifth-order derivative Gaussian pulse fulfills the requirement of the power spectrum density for UWB wireless systems while also maximizing bandwidth. The structure, function and simulation of the pulse generator are introduced in chapter 3. In chapter 4, we focus on the pulse shaper FIR filter. In this section, we also discuss the Parks-McClellan algorithm which is used to design and optimize a FIR filter. The simulation result of the impulse generator is discussed in chapter 5. Finally, in chapter 6, the conclusion and future work are introduced.

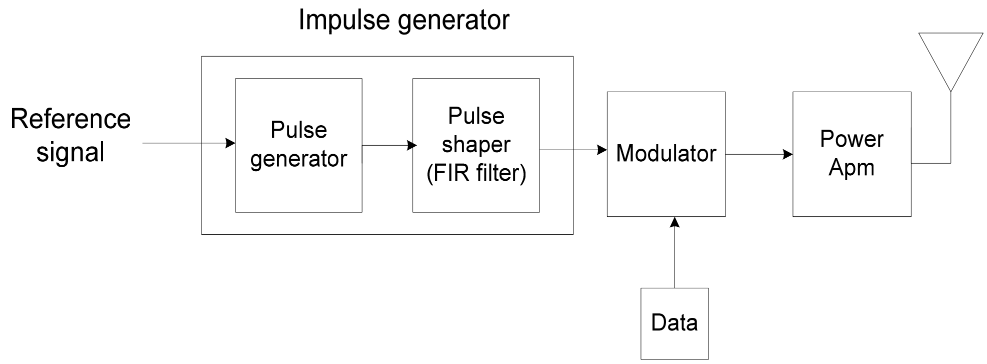

Figure 1.1 The functional block diagram of a typical pulsed UWB transmitter

CHAPTER 2

BACKGROUND

2.1 UWB Communication System

Impulse radio Ultra-wideband (UWB) is a very promising new technology that has the potential to revolutionize wireless communications. It operates using low power ultra-short information bearing pulses. In this section, we will introduce the IR-UWB system including its definition, advantages, applications, pulses, and the types of modulation.

2.1.1 The Definition of UWB

The most frequent use of the term “Ultra-wide bandwidth (UWB)” comes from the UWB radar world and refers to electromagnetic waveforms. Those are characterized by an instantaneous fractional energy bandwidth which should be greater than about 0.20-0.25. To understand this definition, first consider the definition of the energy bandwidth of the waveform. Let E be the instantaneous energy of the waveform; the energy bandwidth is then identified by the frequencies f_L and, which set the limits of the interval where most of E (say over 90%) falls. We call the f_L - f_H width of the interval the energy bandwidth, and the center frequency $(f_L + f_H)/2$ as showing in (Figure 2.1) [17].

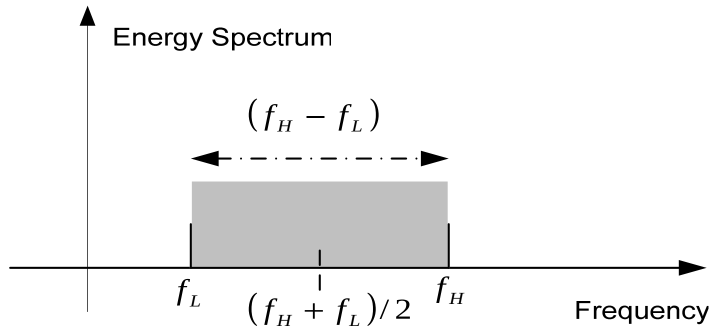

Figure 2.1 Energy bandwidth

Ultra-Wideband characterizes transmission systems with instantaneous spectral occupancy in excess of 500 MHz or the fractional bandwidth of more than 20%. The fractional bandwidth is defined as B / f_C, where B = f_H – f_L denotes –10dB bandwidth and center frequency f_C = (f_H + f_L) / 2 f_L with being the lower frequency of the –10dB emission point (Figure 2.2).

According to FCC regulations, UWB systems with f_C >2.5 GHz need to have a –10 dB bandwidth of at least 500 MHz, while UWB systems with f_C <2.5 GHz need to have fractional bandwidth at least 0.2 [1].

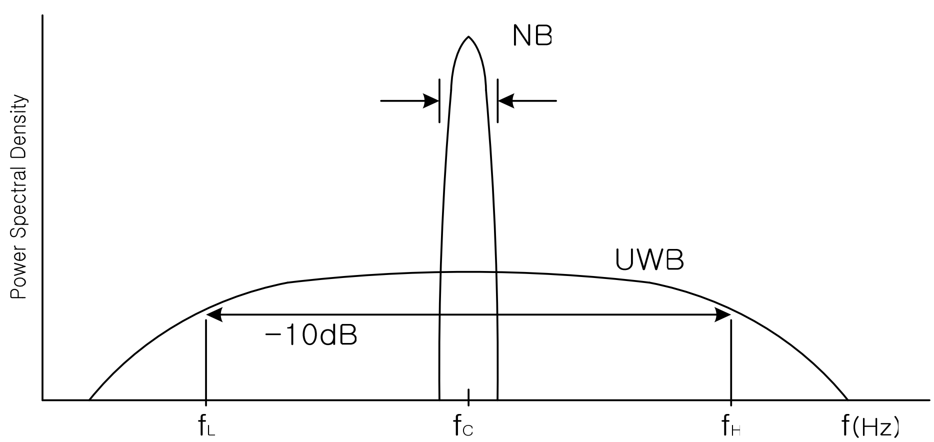

Figure 2.2 UWB bandwidth

2.1.2 FCC Regulation

In 1998, FCC began the process of UWB technology regulatory review. In February 2002, FCC made the formal rule that permits Ultra Wideband to operate under certain indoor and outdoor power spectral masks. In this thesis, the indoor power spectral mask will be discussed.

The Figure 2.3 shows the operating and FCC acceptable frequency range of some high frequency services. Most high frequency cases are regulated by FCC Part 15. Of course, UWB systems including wireless communications are defined in this. According to Figure 2.3, UWB wireless communication systems must operate at above 3.1 GHz and with less than -40dBm of EIRP, which stands for Equivalent Isotropically Radiated Power, which means the signal power supplied to the UWB antenna.

The center frequency is defined as,

$$f_C = \frac{(f_H + f_L)}{2} \tag{2-1}$$

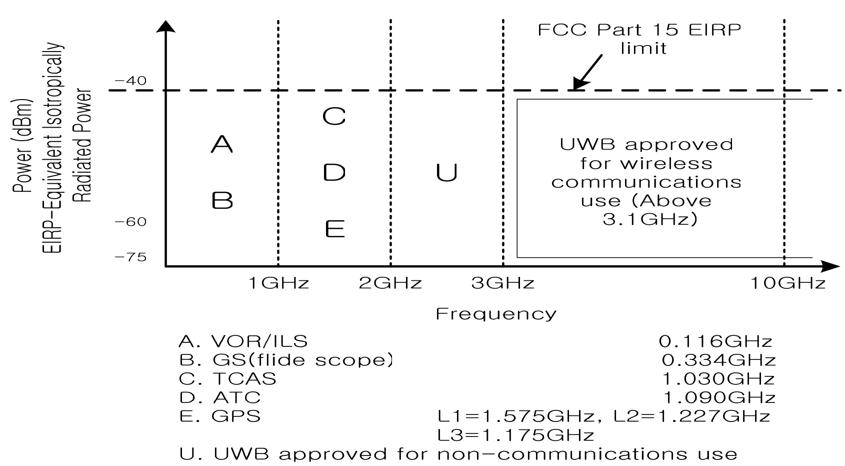

Figure 2.3 FCC part 15 for high frequency devices

As shown in Figure 2.4, for indoor applications, the emission power of UWB devices should be below -41.3 dBm/MHz from 0 Hz to 0.96 GHz, below -75.1 dBm/MHz from 0.96 GHz to 1.61 GHz, below -53 dBm/MHz from 1.61 GHz to 1.99 GHz, below -51.3 dBm/MHz from 1.99 GHz to 3.1 GHz, below -41.3 dBm/MHz from 3.1 GHz to 10.6 GHz, and below -51.3 dBm/MHz from 10.6 GHz above.

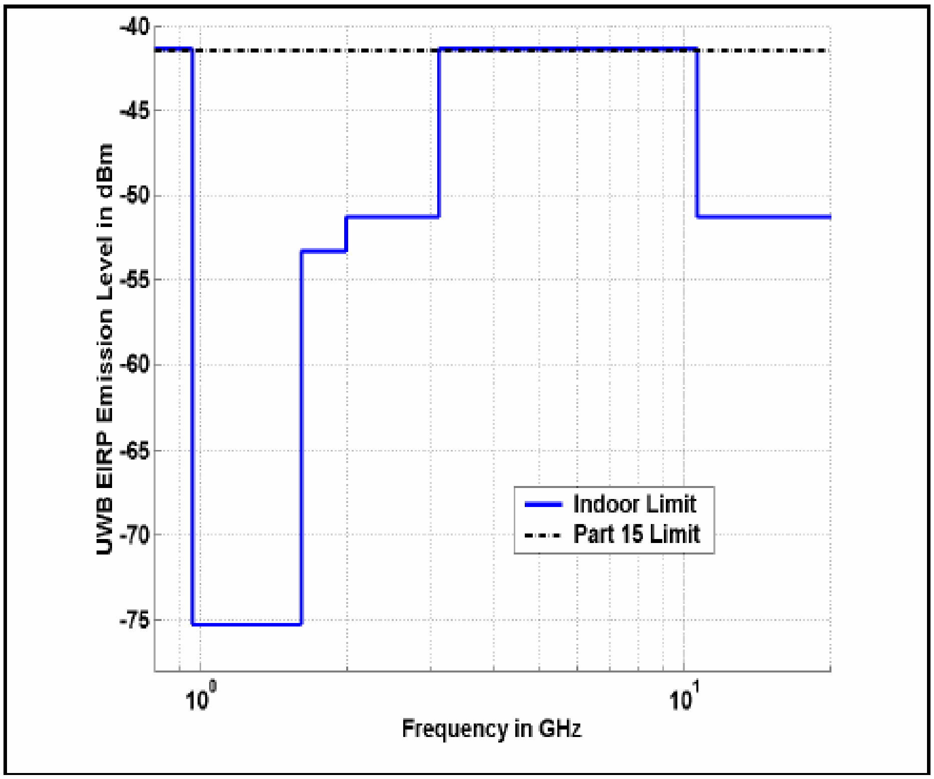

Figure 2.4 FCC spectral mask for UWB communication systems [21]

2.1.3 Advantages of UWB Communication System

Since UWB is based on the transmission of extremely narrow pulses with a small amount of power, UWB communication system have certain advantages over narrow band communication systems. UWB schemes can achieve very high data rates over short distances. According to Shannon's communication theory,

$$C_C = W \log_2 (1 + \frac{S}{N}) \tag{2-2}$$

(Cc is channel capacity, W is bandwidth, S is average transmitted signal power, and N is average noise power), the information capacity increases linearly with frequency bandwidth, and increases logarithmically with the signal to noise ratio. Since Ultra wideband has wide bandwidth, it is suitable for high data rate communication. The data rate of UWB as define by IEEE 802.15.3a proposals can achieve up to 480Mbps. This data rate is far beyond the existing 1 Mbps of Bluetooth, 11 Mbps of 802.11b, and 54 Mbps of 802.11a/g.

In a multipath dominated environment, such large transmission bandwidths allow for fine time resolution of multipath arrivals, which implies potential for reduced fading compared with the narrower bandwidth [16]. Since the transmitter and receiver work in high resolution time domain, each multi path signal can be detected as an individual signal, i.e. without fading. Due to its fine range resolution, UWB technology can also be applied to location-aware wireless networking. In wall penetrating radar, UWB signals can precisely track moving objects behind the wall. In addition, very low power and high processing gain will enable overlay and ensure only minimal mutual interference between UWB and other applications.

Another advantage of UWB is low cost. Since impulse radio is carrier-less, and it only has base-band processing, there is no intermediate frequency (IF) processing needed. That is, resulting in simpler circuitry. Their low cost is due to the fact that UWB devices do not require LO and up- or down- converters.

2.1.4 Applications of UWB Communication Systems

Based on the above advantages, the potential of UWB systems is vast. Popular applications of UWB can be categorized into four categories, i.e., Wireless personal area networks (WPANs), Sensor networks, imaging systems, and vehicular radar systems.

Wireless personal area networks (WPANs), attend to short-range (generally within 10−20 m) ad hoc connectivity among portable consumer electronic and communication devices. They are predicted to provide high-quality real-time video and audio distribution, file exchange among storage systems, and cable replacement for home entertainment systems. UWB technology comes out as a promising physical layer candidate for WPANs, because it presents high-rates over short range, with low cost, high power efficiency, and low duty cycle [1].

Sensor networks consist of a large number of nodes which spread across a geographical area. The most important requirements for sensor networks operating in challenging environments include low cost, low power, and multi-functionality. High data-rate UWB communication systems are well suited for gathering and disseminating or exchanging a vast quantity of sensory data in a timely manner. Typically, energy is more limited in sensor networks than in WPANs. In addition, using the precise localization capability of UWB promises wireless sensor networks with improved positioning accuracy. This is especially useful when GPS is not available, e.g., due to obstruction [1].

UWB-based imaging systems differ from conventional radar systems where targets are typically considered as point scatterers, because UWB radar resolution is shorter than the target dimensions. UWB reflections from the target exhibit not only changes in amplitude and time shift but also changes in the pulse shape. As a result, UWB waveforms exhibit distinct sensitivity to scattering relative to conventional radar signals. This property has been readily adopted by radar systems and can be extended to additional applications, such as underground, through-wall and ocean imaging, as well as medical diagnostics and border examination devices [1].

Vehicular radars use the frequency band surrounding 24 GHz to measure the location and movement of objects around a vehicle by transmitting UWB pulses and detecting the reflected signals. These devices allow the features such as auto navigation, collision avoidance, improved airbag activation, and intelligent suspension systems, etc [1].

2.2 Gaussian Pulse Types and Modulation

2.2.1 Gaussian Pulse Types

Impulse Radio is one of the popular choices for UWB transmission. Since it does not use a sinusoidal carrier to shift the signal to a higher frequency but instead communicates with a baseband signal composed of subnanosecond pulses. Because of the short duration of the pulses, the spectrum of the UWB signal can be several gigahertzes wide. For an UWB communication system, one of the most important design considerations is the selection of the fundamental pulse shape used to generate the UWB signal [3].

A Gaussian pulse (Figure 2.5) is one candidate for the monocycle in UWB impulse radio systems. If a Gaussian pulse is sent to the antenna, the antenna modifies the pulses such that the output of the transmitter antenna can be modeled by the first derivative of the Gaussian pulse. However, the standard monocycles do not satisfy the FCC spectral rules (Figure 2.6).

The PSD of the transmitted signal, P(f) is

$$P(f)=\frac{\sigma_a^2}{T}\left|Y_n(f)\right|^2+\frac{\mu_a^2}{T^2}\sum_{k=-\infty}^{\infty}\left|Y_n\left(\frac{k}{T}\right)\right|^2\delta\left(f-\frac{k}{T}\right) \qquad (2\text{-}3)$$

$Y_n(f)$: the Fourier transform of the n-th derivative of Gaussian pulse;

$\sigma_a^2 \quad and \quad \mu_a$: variance and mean

$\delta(\cdot)$: Dirac delta function

Gaussian pulse:

$$y(t)=\frac{A}{\sqrt{2\pi}\sigma}\exp\left(-\frac{t^2}{2\sigma^2}\right), \qquad (2\text{-}4)$$

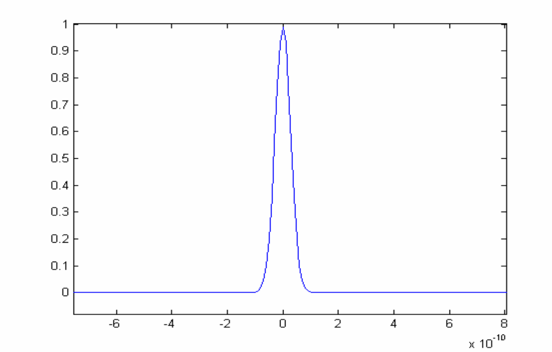

Figure 2.5 Gaussian pulse

In the time domain, the higher-order derivatives of the Gaussian pulse are similar to sinusoids modulated by a Gaussian pulse-shaped envelope. As the order of the derivative increases, the number of zero crossings in time also increases; more zero crossings in the same pulse width correspond to a higher “carrier” frequency sinusoid modulated by an equivalent Gaussian envelope. It means taking the derivative will increase the center frequency of the pulse. These observations guide to considering higher-order derivatives of the Gaussian pulse as candidates for UWB transmission. Specifically, by choosing the order of the derivative and a suitable pulse width, we can find a pulse that satisfies the FCC’s mask. The following paragraph illustrates the spectrum of the higher-order derivatives of the Gaussian pulse and then chooses a pulse shape that meets the emission requirements [4]. The 1st, 2nd, 3rd, 4th, and 5th derivative Gaussian pulses and their PSD will be described in the following.

If the transmitter produces a Gaussian pulse, the output of the transmitter antenna will be the first derivative Gaussian pulse, given by:

$$y^{(1)}(t) = -\frac{At}{\sqrt{2\pi}\sigma^{3}} \exp\left(-\frac{t^{2}}{2\sigma^{2}}\right) \tag{2-5}$$

The PSD of the first derivative Gaussian pulse is shown in (Figure 2.6)

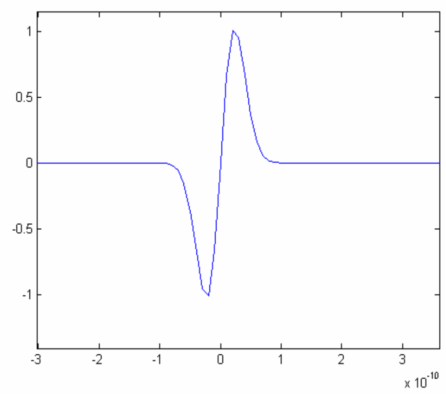

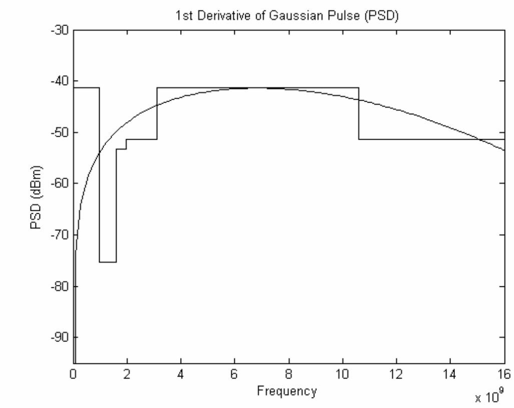

(a) (b)

Figure 2.6 (a) The first derivative Gaussian pulse and (b) PSD

If the transmitter produces a first derivative Gaussian pulse, the output from the antenna will be a second derivative Gaussian pulse, given by

$$y^{(2)}(t) = A\left(\frac{t^2}{\sqrt{2\pi}\sigma^5} - \frac{1}{\sqrt{2\pi}\sigma^3}\right)\exp\left(-\frac{t^2}{2\sigma^2}\right) \tag{2-6}$$

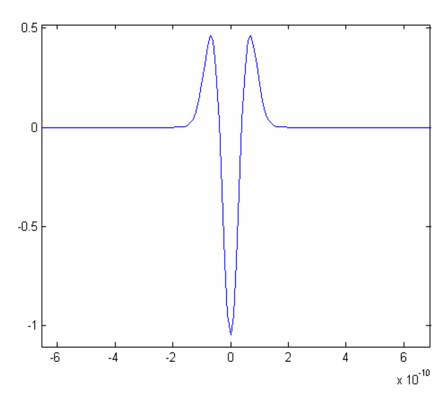

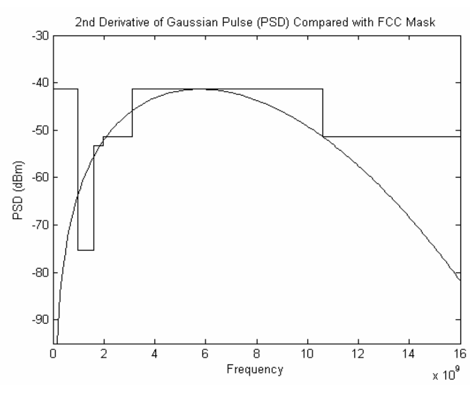

(a) (b)

Figure 2.7 (a) The second derivative Gaussian pulse and (b) PSD

If the transmitter produces a second derivative Gaussian pulse, the output from the antenna will be a third derivative Gaussian pulse, given by

$$y^{(3)}(t) = -A\left(\frac{t^3}{\sqrt{2\pi}\sigma^7} - 3\frac{1}{\sqrt{2\pi}\sigma^5}\right)\exp\left(-\frac{t^2}{2\sigma^2}\right) \qquad (2\text{-}7)$$

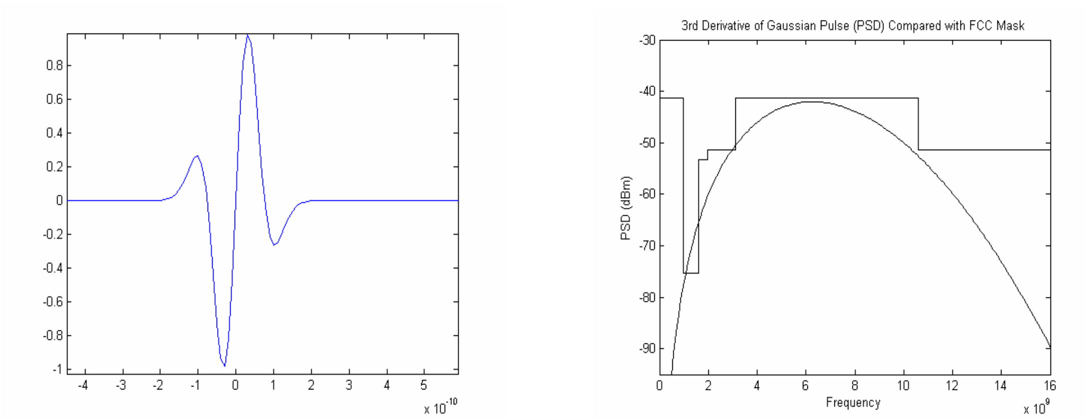

(a) (b)

Figure 2.8 (a) The third derivative Gaussian pulse and (b) PSD

If the transmitter produces a third derivative Gaussian pulse, the output from the antenna will be a forth derivative Gaussian pulse, given by

$$y^{(4)}(t) = A\left(\frac{t^4}{\sqrt{2\pi}\sigma^9} - 6\frac{t^2}{\sqrt{2\pi}\sigma^7} + 3\frac{1}{\sqrt{2\pi}\sigma^5}\right)\exp\left(-\frac{t^2}{2\sigma^2}\right) \qquad (2\text{-}8)$$

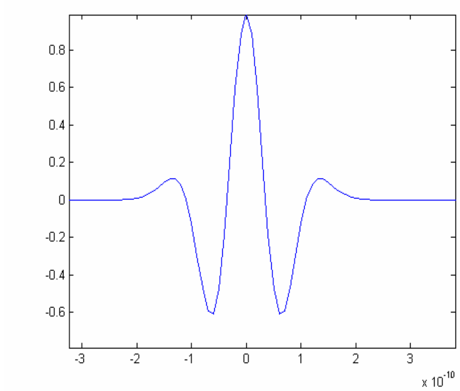

(a)

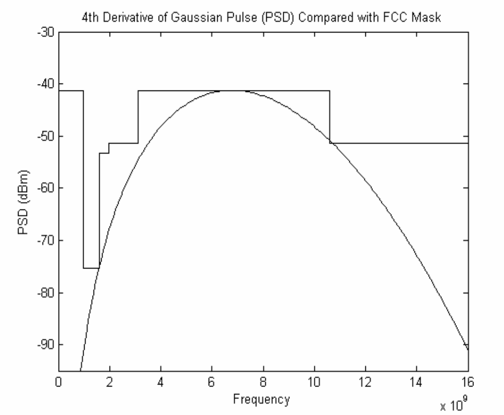

(b)

Figure 2.9 (a) The forth derivative Gaussian pulse and (b) PSD

If the transmitter produces a forth derivative Gaussian pulse, the output from the antenna will be a fifth derivative Gaussian pulse, given by

$$y^{(5)}(t) = A\left(-\frac{t^5}{\sqrt{2\pi}\sigma^{11}} + \frac{10t^3}{\sqrt{2\pi}\sigma^9} - \frac{15t}{\sqrt{2\pi}\sigma^7}\right)\exp\left(-\frac{t^2}{2\sigma^2}\right) \qquad (2\text{-}9)$$

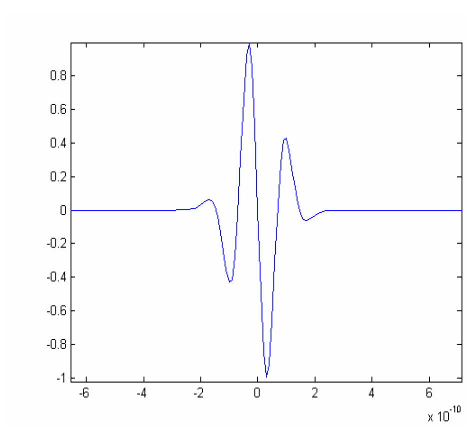

(a)

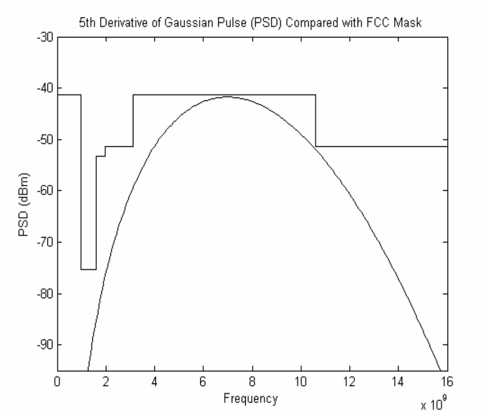

(b)

Figure 2.10 (a) The fifth derivative Gaussian pulse and (b) PSD

Putting the PDS of the 1~5th derivative of Gaussian Pulse to compare, the higher derivative of the Gaussian, the center frequency moving higher and the bandwidth is smaller (Figure 2.11).

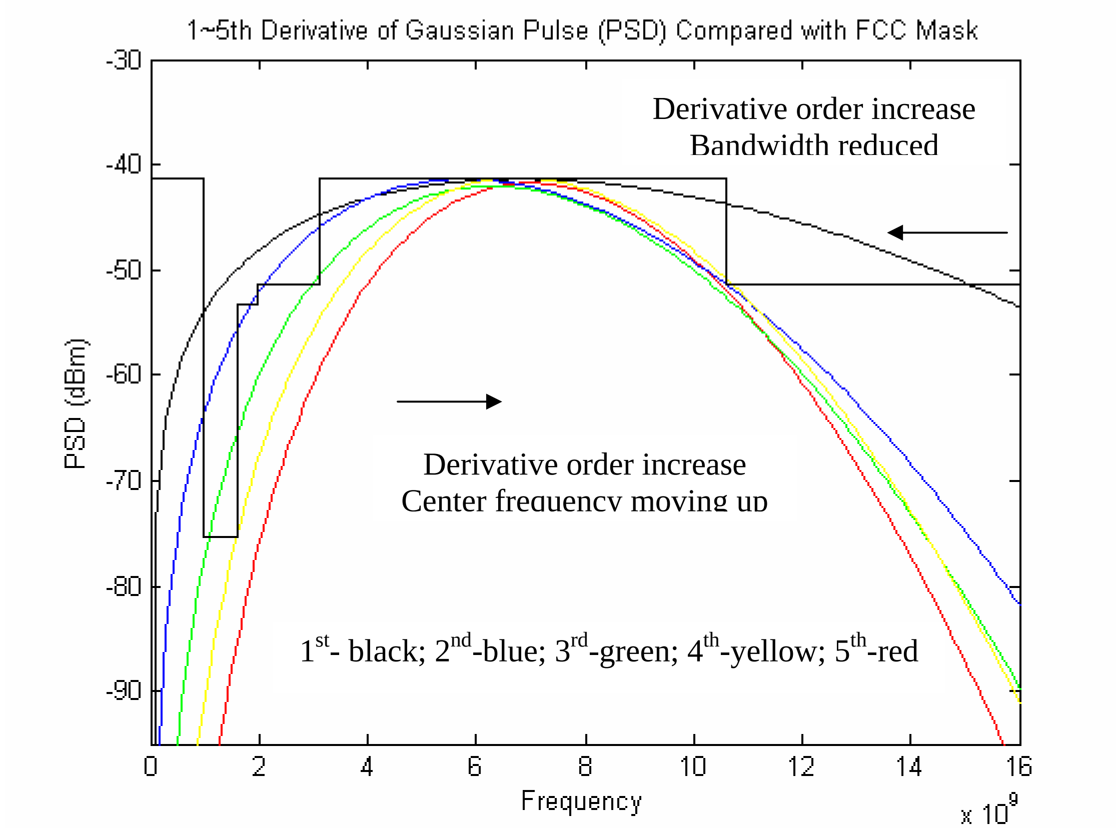

Figure 2.11 The PSD of the 1st to the 5th derivative Gaussian pulses

The FCC issue UWB emission limits in the form of a spectral mask for indoor system. In the band from 3.1 GHz to 10.6 GHz, UWB can use the FCC Part 15 rules with a peak value of -41dBm/MHz. The above simulation results tell us that the PSD of the 5th derivative Gaussian pulse meet the FCC mask.

For the indoor system, at least the fifth-order derivative should be used. The fifth derivative Gaussian also maintains the bandwidth as wide as possible. Although after the 5th derivative pulse has been generated, it will go through antenna twice. It means the 5th pulse at the receiver becomes a 7th derivative pulse. The 7th and 5th derivative pulse are very similar, and also the PDS of 7^{th} derivative pulse is more confident the within the FCC regulation, so generating 5^{th} pulse for communication is necessary.

2.2.2 Pulse Modulation

In UWB communication system, there is variety of modulation types used. Some of them modulate information bits directly into very short pulses. Since there is no IF (intermediate Frequency) processing in such systems, they are often called base-band processing, or impulse radio systems. In the most common approach, the encoded data symbols introduce a time dither on generated pulses leading to the so-called Time-Hopping UWB (TH-UWB). Well-known modulation types include time hopping pulse position modulation, time hopping pulse amplitude modulation, and direct sequence pulse amplitude modulation. On the other hand, some UWB systems do have carriers. For example, in the orthogonal frequency division multiplexing (OFDM) system, the information bits are modulated into orthogonal carriers [14]

2.2.2.1 Impulse Radio System

Time hopping pulse position modulation, time hopping pulse amplitude modulation, and direct sequence pulse amplitude modulation will be introduced in this section.

Time-hopping pulse position modulation (TH-PPM) impulse radio is built upon the time shift of pulses with a certain shape. A UWB system with TH-PPM could accommodate multiple users simultaneously through code division multiple access. In TH-PPM UWB system, the impulse radio signal from the k-th transmitter is generally expressed as [14]:

$$s(t)=\sum_{i=0}^{\infty}\sum_{j=-\infty}^{+\infty}\delta\left(t-jT_f-c_{kj}T_c-iT_b-b_i\Delta\right)\otimes g(t) \tag{2-10}$$

In equation (2.10), notation g (t) denotes the transmission pulse shape function, notation $\otimes$ represents the convolution operation, and the delta function, δ (t), is defined as:

$$\begin{cases}\delta(t)=1, & t=0\\ \delta(t)=0, & t\neq 0\end{cases} \tag{2-11}$$

The term δ ($t–jT_f-c_{kj}Tc-iT_b-b_i\Delta$) $\otimes$ g (t) indicates that the j-th pulse transmitted by the k-th user starts at time period ($t–jT_f-c_{kj}Tc-iT_b-bi\Delta$). In Equation (2-10), the sequence set {c_{kj}} is a pseudo-random time-hopping sequence for user k, and the range of c_{kj} is between 1 and the number of hopping positions, N_k. In multiple-access systems, each user has a separate pseudorandom sequence to distinguish one from the others. Notation T_c is the chip duration and T_f is the frame duration, which is greater than or equal to N_k T_c. The ratio of N_k T_c over T_f, i.e., $R_{frac}=N_kT_c/T_f$, represent the fraction of time over which time hopping sequence occupies [14].

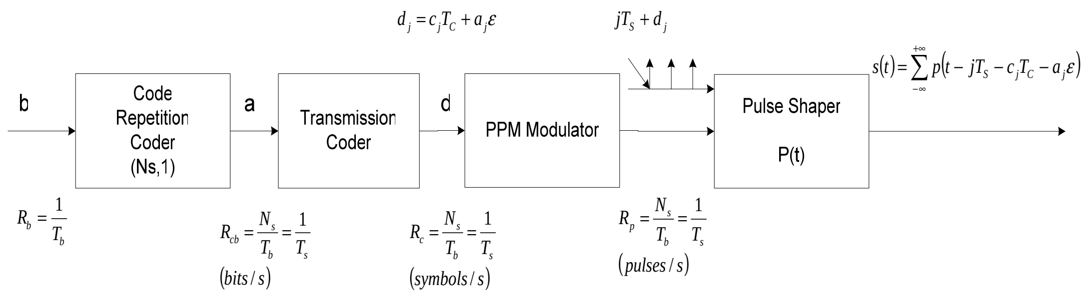

Figure 2.12 Transmission scheme for a PPM-TH-UWB signal [17].

Time hopping binary pulse amplitude modulation (TH-BPAM) is another type of UWB modulation. The pulse amplitude of information bit 1 is set to unit, while the pulse amplitude of information bit 0 is set zero. By setting the pulse on and off, binary information bits, 0 and 1, are sending out. Similar to TH-PPM, the TH-BPAM signal from the k-th transmitter is expressed in equation (2-10), where notation bi denotes the i-th binary sequence bit [14].

$$s(t) = \sum_{i=0}^{\infty} \sum_{j=0}^{N_s - 1} \delta\left(t - jT_b - jT_f - c_{k,j} T_c\right) \otimes g(t) * b_i \tag{2-12}$$

Direct sequence binary pulse amplitude modulation (DS-BPAM) UWB signal can be expressed in equation (2-12), in which the spreading sequence takes on 0 or 1 and is multiplied into signal amplitude [14].

$$s(t) = \sum_{i=0}^{\infty} \sum_{j=0}^{N_s - 1} \delta\left(t - jT_b - jT_c\right) \otimes g(t) * c_{k,j} * b_i \tag{2-13}$$

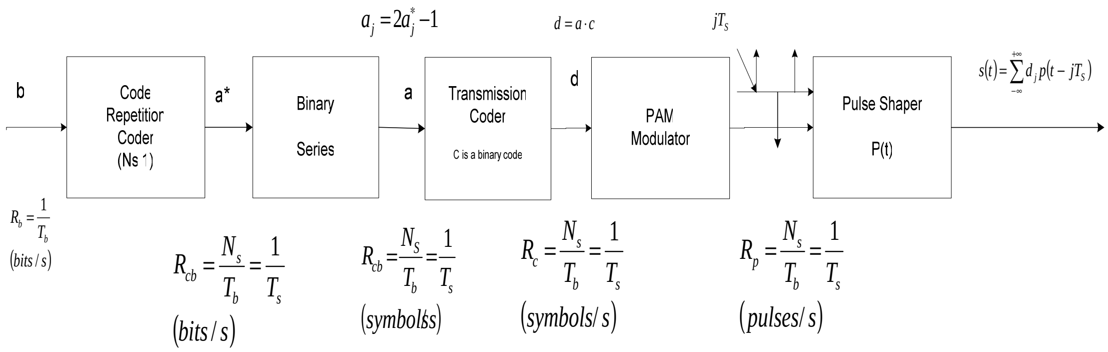

Figure 2.13 Transmission scheme for a PAM-DS-UWB signal [17].

2.2.2.2 Orthogonal Frequency Division Multiplexing

Orthogonal Frequency Division Multiplexing (OFDM) modulation can also be used in UWB communication systems. In OFDM communication systems, the orthogonal sub-carriers can make sure that sub-carriers do not interfere with each other, so the internal inter-carrier interference is negligible. Moreover, the external narrowband interference will affect at most a couple of sub-carriers and information from the affected sub-carriers can be erased and recovered via the forward error correction (FEC). Therefore, OFDM has an inbuilt robustness against interference. In general, two complex signals, $X_1(t)$ and $X_2(t)$, on some time interval [a, b], are defined as orthogonal if and only if they satisfy the following condition

$$\int_a^b x_1(t) x_2^*(t) dt = 0 \tag{2-14}$$

Let's define the symbol rate as f_0, and symbol period as T. If the frequency of each sub-carrier f_c is multiple times of symbol rate f_0, i.e., $f_c = nf_0$ then equation (2-15) happens to hold [14].

$$\int \cos(2\pi n f_0 t) \times \cos(2\pi m f_0 t) dt = 0 \qquad (n \neq m)$$
(2-15)

In other words, sub-carriers nf_0 and mf_0 are orthogonal, when n and m are different. The core of OFDM is to take advantage of this good property of orthogonal sub-carriers by using the inverse discrete Fourier transform (IDFT) in the modulator and discrete Fourier transform (DFT) in the demodulator [17].

In OFDM modulator, there are totally N sub-carriers, among which N_u sub-carriers are active and the rest are inactive. The inactive sub-carriers are set to zero in order to shape the power density spectrum of the transmitted signal. The binary information data are mapped onto the active sub-carriers. The sub-carrier l of the OFDM symbol k is modulated with the complex coefficient A_{kj}. The sub-carrier coefficient vector of symbol k, $A_k = [A_{k,0.} \cdots A_{k,N-1}]$ is then transformed into time domain using a N-point IDFT, i.e., a_k = IDFT [A_k]. In the time domain, the coefficient vector a_k can be calculated following equations (2.16) and (2.17)

$$a_k = \lfloor a_{k,0} \cdots a_{k,N-1} \rfloor$$
(2-16)

$$a_{kj} = \frac{1}{\sqrt{N}} \sum_{m=0}^{N-1} A_{k,m} e^{j\frac{2\pi}{N}mk} \qquad (0 \leq l < N)$$
(2.17)

The samples a_{kj} are transmitted using pulse amplitude modulation. The signal transmitted in time domain is expressed as

$$S(t) = \sum_{k=0}^{\infty} \sum_{j=0}^{N-1} a_{kj} * w(t - kT_{symbol})$$
(2.18)

The symbol period T_{symbol} is N times sample period T_{sample}, i.e., T_{symbol} = N T_{sample}. Notation w (t) is a rectangular pulse of symbol duration T_{symbo}.

In contrast to conventional frequency shift keying, the spectral overlapping among sub-carriers is allowed in OFDM since orthogonality will ensure the sub-carrier separation in the receiver. This leads to better spectral efficiency of OFDM. Since the use of steep band-pass filter is eliminated, the cost of OFDM system is also reduced. The OFDM symbol period is longer than the propagation channel delay spread, and this results in flat fading channel for each sub-carrier, which can be easily equalized if it is necessary [17].

The multi-band approach breaks the 7.5 GHz of available spectrum into 15 subbands. Such a method provides great spectral efficiency, utilizing the entire available bandwidth. By using many different subbands, the system can easily co-exist worldwide, by simply turning off some sub-bands that might interfere with other devices. Another advantage of a multi-band approach is its ability to efficiently capture multipath energy without fading [17].

2.2.2.3 OFDM vs IR

Table 2.1 The Comparison OFDM and IR

	MB-OFDM	IR-UWB
Bandwidth (main different):	• The spectrum is divided into sub bands of approximately 500 MHz each. • (Multi - Band)	• Using all of the available bandwidth • (Single - Band)
Speed	• Texas Instruments OFDM: Reaching a maximum speed of 480 Mb/s.	Motorola's proposal used DS-UWB: Improving the effect of timing jitter like ISI and allows them to reach speed beyond 1Gbps.
Carrier	• Carrier based	• Non – Carrier based
Power Consumption	• More Power consumption	• Less Power consumption
System Complexity	• More Complex • Need Up / Down converter • DAC after Baseband	• Less Complex • No Up / Down Converter • No DAC after Baseband
Peak-to-average power ratio (PAR):	• Very high PAR: interference with other systems if they both operate in the same band.	• Very low PAR:
Antenna	• Wideband Matching	• Wideband Matching • Additional Derivation can change the signal type

2.3 MOS Curent Mode Logic (MCML)

MOS Current Mode Logic (MCML) is studied for low power, high speed and mixed signal environment. Since it has lower output swing than CMOS, MCML has lower power consumption and high speed. If CMOS circuits switch frequently, the power consumed from dynamic circuit power consumption becomes the main part, thus

MCML circuit's small voltage swing enables MCML to dissipated less power than CMOS. For mixed signal environments, the constant current supplied by Vdd is extremely desirable. Since the MCML is a differential logic style, the PDN is fully differential, the dI/dt effects are negligible in comparison to CMOS circuits and the current variation is hypothetically 0 [26].

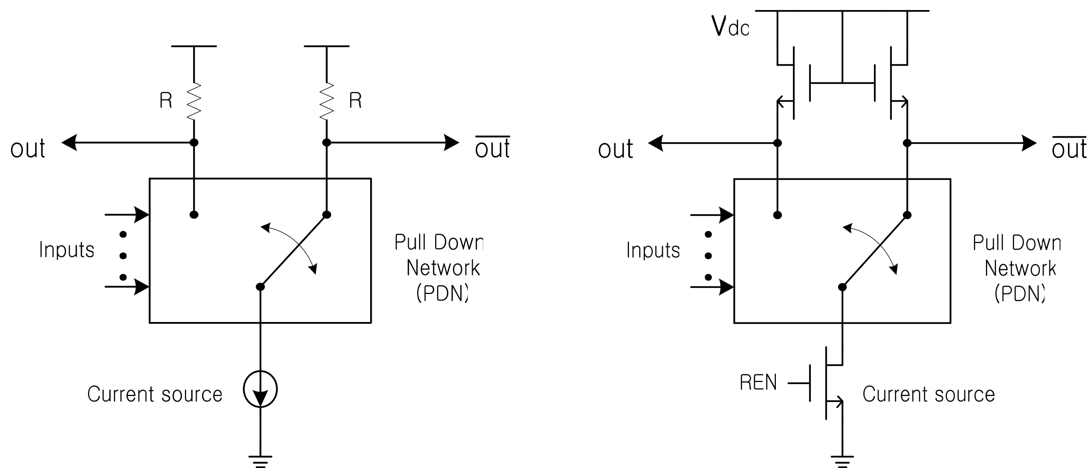

(a) (b)

Figure 2.14 Simple MCML block and simple CMOS block
(a) passive load and (b) active load

The basic CML structure contains three mail blocks: differential pull down network (PDN), pull up resistor, and current source. The inputs to the pull down network are fully differential. In MCML circuits the pull down network is regulated by a constant current source. The pull down network steers the current I to one of the pull up resistors based upon the logical function being implemented. The resistor connected to the current source through PDN will have current I and a voltage drop $\Delta V = I \times R$.

The other resistor will not have any current flowing through it and its output node will be pulled up to VDD in the DC state. If we look at the different output voltage, the voltage swing is set exclusively by the amount of current (I) and the value of the pull up resistance (R). The output swing is generally much smaller than VDD, of the order of a few hundred millivolts.

The PDN switch is implemented with a standard nMOS differential pair controlled the signal input. The current source is an nMOS device with a constant gate voltage (RFN) making the nMOS in the saturation region. The load resistor is pMOS devices with fixed gate voltages (RFN) and is designed to be operated in the linear region in order to model resistor (Figure 2.14) [26]. Current I flow through the transistor which has the same R, and then the voltage drop ΔV is transferred to the output node. The total voltage swing is also ΔV, which is set by adjusting the resistance of the pull-up devices for a given current. In this case, ideally, the other resistor will not have any current flowing through it and will be pulled up to Vdd. In reality a current always flows in both the resistors because the transistors are always ON (fully or partially).[26] So, in this thesis, all load pMOS transistors were replaced by nMOS transistors with the same function in order to achieve faster output response and better flexibility in MOS size changing (Figure 2.14).

2.3.1 MCML Delay and Power Dissipation

Assume that our circuit is a linear chain of N identical gates, all with load capacitance C and voltage swing ΔV. The relationship between current and the capacitance is

$$I = C\frac{dv}{dt}.$$

The total propagation delay of N:

$$Delay_{MCML} = N \times R \times C = \frac{N \times C \times \Delta V}{I} \tag{2-19}$$

where N is the total logic depth of the circuit.

Therefore, the delay can be adjusted through ΔV and the bias current I. We adjust these two parameters to obtain the necessary delay in our design. Due to a constant current source, the static power consumption of an MCML circuit can be calculated as follows:

$$Power = N \times I \times Vdd \tag{2-20}$$

While static CMOS gates tend to dissipate static and dynamic power, the current draw of MCML gates is independent of switching activity. With this assumption, we can write expressions for power, power-delay, and energy-delay:

$$P_{MCML} = N \times I \times V_{dd} \tag{2-21}$$

$$PD_{MCML} = NIV_{dd} \times \frac{NC\Delta V}{I} = N^2 \times C \times \Delta V \times V_{dd} \tag{2-22}$$

$$ED_{MCML} = N^2 C\Delta V V_{dd} \times \frac{NC\Delta V}{I} = \frac{N^3 \times C^2 \times \Delta V \times V_{dd}}{I} \tag{2-23}$$

The delay, power, power-delay, and energy-delay for static CMOS logic are well known and approximated by [26]:

$$D_{CMOS} = \frac{N \times C \times V_{dd}}{\frac{k}{2} \times (V_{dd} - V_t)^{\alpha}} \tag{2-24}$$

$$P_{CMOS} = N \times C \times V_{dd}^2 \times \frac{1}{D_{CMOS}} \tag{2-25}$$

$$PD_{CMOS} = N \times C \times V_{dd}^2 \tag{2-26}$$

$$ED_{CMOS} = N^2 \times 2 \times \frac{C^2}{k} \times \frac{V_{dd}^2}{(V_{dd} - V_t)^{\alpha}} \tag{2-27}$$

where k and α are process and transistor size dependent parameters. In real MCML design, designers also have some more properties have to be considered. The logic depth, N, and voltage swing range are very important factors for real design. According to the equations provided below, the logic depth, N, is very seriously related to the performance of MCML operation. In high speed applications, the most critical benefit of MCML is lower power consumption than CMOS logic even though this MCML consumes more power at slow operation. So, keeping the N as small as possible has to be reminded for designers in order to have desired performance in power consumption with this high CMOS micron technology, which supplies very low power to a circuit. Similarly, the energy-delay is proportional to the square of the voltage swing for MCML. This fact encourages the use very low swing circuits [26].

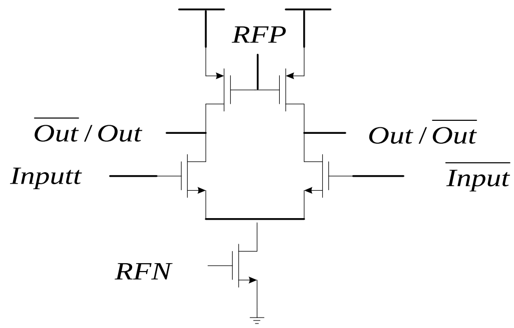

Figure 2.15 Basic MCML inverter / buffer circuit

2.3.2 The comparison MCML and CMOS

Table 2.2 The Comparison MCML and CMOS

CMOS logic	MCML logic
1. It is not suitable for high speed applications. • Turn off and Turn on time limit the maximum speed. • Power consumption increases with frequency. • Each input is connected to at least two gates. • P-type devices play a key role. • Large Voltage swing. • Rate of charge and discharge is not the same.	1. Transistors are always on (fully or partially) • Higher speed. • Low threshold devices can be used. i. Lower Vdd. ii. Lower power dissipation. • Static Power dissipation.

Table 2.2 – continued

2. High Dynamic Power dissipation • Large Voltage Swing • Large supply voltage and large threshold voltage.	2. Smaller swing voltage • Higher speed • Lower dynamic power dissipation. • Lower noise generation. • Lower noise margin
3. CMOS produces lots of noise. • Sharp switching currents. • Voltage Variation.	3. Gates are based on n-type differential pair • Immunity to common mode noise. • Smaller input capacitance. • Transistors have to be identical.
4. CMOS circuits are less robust. • Propagation delay varies with supply voltage. • Propagation delay varies with threshold voltage. • Noise can degrade performance.	4. Gates draw static amount of current from Power supply. • Reduces the amount of spiking of the supply and substrate voltage (lower noise) • Rate of charging and discharging is constant. • Higher degree of freedom to optimize delay/Energy-Delay product.

Table 2.2 – continued

5. CMOS consumes too much area • Pull up network made up of large pMOSs.	5. P-type devices are never used as a switch. • Higher speed • Lower number of transistors.
6. Low degree of freedom in optimization.	

2.4 UWB Transmitter

Impulse radio uses single pulse as a transmission carrier to implement the UWB technology. The function of UWB transmitter is generating and transmitting the very short duration pulse which has very wide bandwidth without carrier as a signal. The general function block of the transmitter is shown in Figure 2.16. Different impulse generators' structures implement as different modulation methods, pulse types, and fabrication technologies. A several systems of impulse generators and generated pulses for UWB communication system will be discussed and as following.

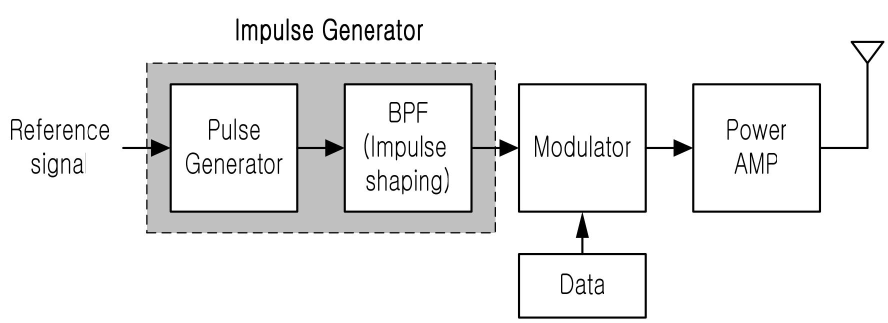

Figure 2.16 Block diagram of a typical pulsed UWB transmitter

2.4.1Background on Different Types of Pulse Generators

There have been several previous attempts at implementing a form of a Gaussian pulse suitable for use in an IR-UWB system. However, none of the previous attempts mentioned generate a type of Gaussian pulse whose PSD conforms to the FCC mask. It has been shown that only the derivatives higher than the 3rd order meet the power spectral density mask mandated by the FCC [11]. Previously designed UWB pulse generators in [2], [13], [18] and [20], generate only the first derivative of the Gaussian pulse, i.e. the Gaussian monocycle. The following paragraph introduces the different transmitters for UWB system.

1. The Intra/Inter-chip Wireless Communication [13]:

Intra/Interchip wireless interconnects systems using integrated antenna is proposed to realize high speed data and clock distribution without any parasitic delay. For high data transmission rate and multiple access capability of this wireless interconnection system, it requires wideband characteristics of integrated transmitter, receiver and antenna. Thus a UWB system appears to have a great potential for implementation of wireless interconnect system for future ULSI.

It uses time hopping impulse radio and the pulse modulation type is PPM The generated pulse type is Gaussian monocycle.

2. A SiGe BiCMOS Ultra Wide Band RFIC Transmitter Design for Wireless Sensor Network [18]:

Wireless sensor networks represent a rapidly emerging technology for commercial, industrial and military systems that include control and monitoring operations.

The wide available bandwidth provides flexibility in sensor applications, where different sensor node could share the same band or hop over different bands depending on their data rates (e.g. high data rate video sensors, medium data rate acoustic sensors, low data rate environmental sensors, etc.).

It uses Frequency hopping technique and the pulse modulation type is BPSK. The generated pulse type is monocycle.

3. An Ultra Wideband TAG Circuit Transceiver Architecture [20]:

Designed for an indoor network with low data rate of the order of l kbps – l0 kbps, low cost, a low power applications, low complexity UWB TAG transceiver with built in location and tracking. Utilizing individual identification of each unit, 1 measurement/second per unit, centralized control and positioning calculation in base stations, operation in unlicensed bands, and two way data transfer sufficient to allow position information to be relayed. This transceiver contains the oscillator, the transmitter, the receiver and baseband digital signal processing (DSP) block.

It is designed in a 0.35 um Si-Ge, BiCMOS process from Austria Microsystems. It uses time hopping direct-sequence technique and the pulse modulation type is BPM. The generated pulse type is monocycle.

4. A Novel CMOS/BiCMOS UWB Pulse Generator and Modulator [19]:

A new low voltage high frequency pulse generation circuit is fully integrated in CMOS and or BICMOS process. Generate symmetrical pulse those are the second-order derivative of Gaussian with a bandwidth up to 5 GHz and having sufficient swing for UWB applications. Based on the proposed pulse generator, a novel BPSK pulse modulator is also proposed and can be directly used in UWB transmitter.

It uses impulse radio time and the pulse modulation type is BPSK. The generated pulse type is 2nd order derivative Gaussian pulse.

5. All-digital low-power CMOS pulse generator for UWB system [11]:

The proposed pulse generator generates a single UWB pulse satisfying FCC regulations without any filtering. The 5th derivative of the Gaussian pulse is a single pulse with the most effective spectrum under the FCC limitation floor, and this pulse can be transmitted without any filtering.

It uses impulse radio technique and the pulse modulation type is BPM. The generated pulse type is 2nd order derivative Gaussian pulse.

6. A PPM Gaussian Pulse Generator for Ultra-Wideband Communications [2]:

The implementation of an active Gaussian pulse generator is the focus on transmitting pulses of ultra-short duration with very low power spectral density, a wide fractional channel bandwidth and excellent immunity to interference from other radio systems.

Gaussian pulses offer an excellent time frequency resolution product. Pulse position modulation is used to encode the binary transmitted data. The Gaussian pulse generator comprises a cascade of a fast triangular pulse generator and a Gaussian filter (i.e., a filter with a Gaussian impulse response). It is central to the ultra wideband transmitter design.

It uses impulse radio technique and the pulse modulation type is PPM. The generated pulse type is monocycle.

Table 2.3 The Summarize of Different UWB Transmitter and Generated Pulse Type

UWB transmitter	Pulse type
COMS UWB transmitter: The Intra/Inter-chip Wireless Communication by: Hiroshima University	Monocycle
A SiGe BiCMOS Ultra Wide Band RFIC Transmitter Design for Wireless Sensor Networks by: Virginia Tech. (fabricated by freescale semiconductor)	Monocycle
An Ultra Wideband TAG Circuit Transceiver Architecture	Monocycle
A Novel CMOS/BiCMOS UWB Pulse Generator and Modulator	2nd order derivative Gaussian pulse
All-digital low-power CMOS pulse generator for UWB system	2nd order derivative Gaussian pulse
A PPM Gaussian Pulse Generator for Ultra-Wideband Communications	Monocycle

Examining some previously designed UWB pulse generators [2], [13], [18], [19], [20] reveal that their generated pulses are not the 5th derivative Gaussian pulse, including the other all-CMOS impulse generators [11]. That is the motivation of generating the 5^{th} Gaussian for UWB indoor communication system.

CHAPTER 3

IMPULSE GENERATOR FOR UWB WIRELESS GENERATOR

In the UWB communication systems, the pulse transmitting block (Figure 1.1) has to generate very short duration impulses before modulating the signal. For this kind of function, this block can be composed of a digital pulse generator and an impulse shaping circuitry (Figure 3.1). In this thesis, the digital transmitter consists of a delay line and a XOR cell, and the impulse shaping circuitry which can be applied by a bandpass filter, FIR filter. The final output shape must be a Gaussian Monocycle pulse, which is the 5th derivative of Gaussian pulse.

To design the pulse generator, delay circuits and XOR circuits have been used. The reference clock signal is sent to the delay circuit, and the delayed signal is applied to the XOR gate with the reference clock signal [6] [7]. In the delay circuit, the delay time is controlled by the voltage. Thus, the delay time can be adjusted from 1.5ps to 36ps. Using the control voltage to adjust the delay time in the delay circuit; the pulse generator can change the pulse width (1/f) to achieve a certain frequency. Appling this delay circuit performs the same function in controlling frequency as an RLC network [8]. The Gilbert Cell is used as an XOR gate to create pulses. The center frequency from the XOR gate is 8GHz. When the two different input signals have opposite levels at the same time into the XOR, short pulses will be generated out from XOR gate. Those short pulses are Gaussian pulses, and then become the input signals to the impulse shaping circuit FIR filter. The FIR filter operates as an impulse shaping circuit based on the primary operation characteristics of convolution. The proposed FIR filter performs a convolution of the filter impulse response with a sequence of input values and produces an equally numbered sequence of output values.

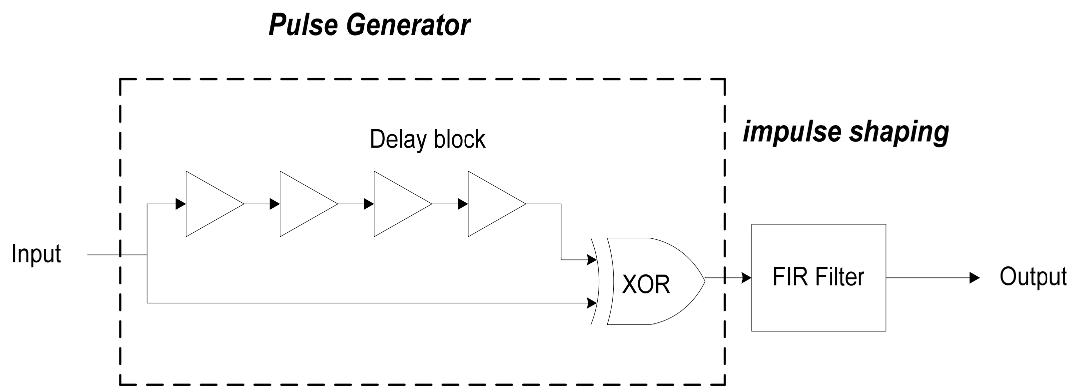

Figure 3.1 Impulse generator block diagram

3.1 Pulse Generation

In a UWB communication system, the pulse generator is the most initial operating block, which includes a delay line and XOR gate before the shaped impulse generated. It deals with an original input signal and also the delays the signal through the delay line in order to detect the opposite input levels in the same time (Figure 3.2). So this block actually works like a phase detector. When the two different inputs digital signals have opposite phase, like 1 or 0 and 0 or 1, which arrive at the XOR gate at the same time, the pulse generator generates pulses as Figure 3.3 showing.

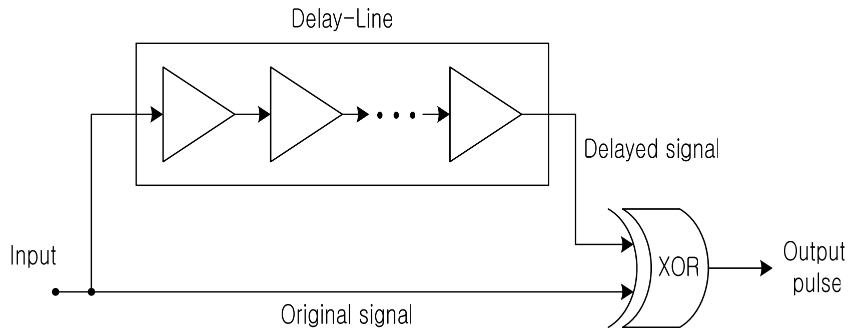

Figure 3.2 Pulse generation block diagram

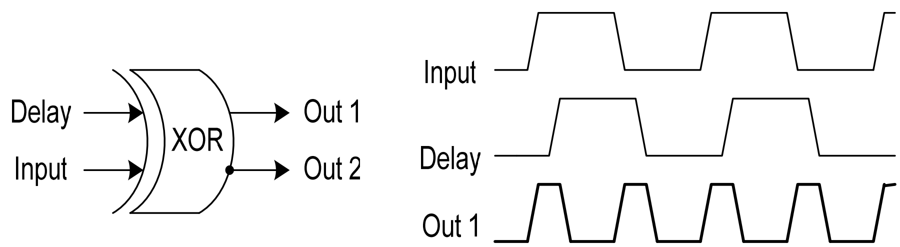

Figure 3.3 Pulse generation output signals

The following subsection will introduce the operation and simulation of each block.

3.1.1 Variable Delay Circuit

In a high-speed communication system, in order to perform a delay line for signal transmitting block, the "interpolation" is usually achieved by its actual shifting delay output ability. Instead of laying down the slope of a delayed signal by changing the current, the variable delay circuit combines of two different speeds of delay paths as Figure 3.4 showing.

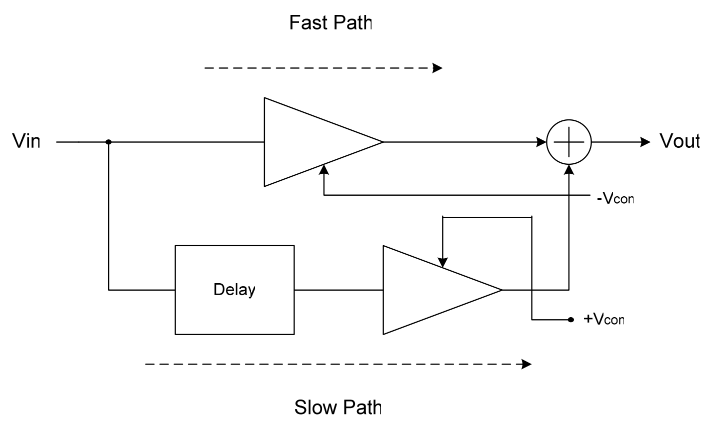

Figure 3.4 Interpolation delay stage block with variable control used in this thesis

This delay stage consists of a fast path, which is a single differential pair and a slow path which is two differential pairs in series. The same input signal comes into both paths, and then their outputs are combined. Those gains of each path are adjusted by V_{cont} in opposite directions. At one extreme of the control voltage, only the fast path is on and the slow path is disabled. Conversely, at the other extreme, only the slow path is on and the fast path is off. If V_{cont} lies between the two extremes, each path is partially on and the total delay is a weighted sum of their delays [8].

Each stage can be simply realized as a differential pair. The gain is controlled by its tail current. Since the two transistors in a differential pair provide separate output currents, the outputs of the two pairs can be added in the current domain. Simply shorting the outputs of two pairs performs the current addition, e.g., for small signals,

$$I_{out} = g_{m1,2}V_{in1} + g_{m3,4}V_{in2} \tag{3-1}$$

The overall interpolating stage therefore assumes the configuration shown in Figure 3.5, where V^{+}_{con} and V^{-}_{con} denote voltages that vary in opposite directions (so that when one path turns on, the other turns off). The output currents of M_1-M_2 and M_3-M_4 are summed at X and Y. The currents flow through R1 and R2 to produce V_{out} [8].

In the circuit of Figure 3.5, the gain of each stage is varied by the tail current to achieve interpolation, but it is desirable to maintain constant voltage swings. We also recognize that the gain of the differential pair M_5-M_6 need not be varied because even if only the gain of M_3-M_4 drops to zero, the slow path is fully disabled. We then guess that if the tail currents of M_1-M_2 and M_3-M_4 vary in opposite directions such that their sum remains constant, we achieve both interpolation between the two paths and constant output swings [8].

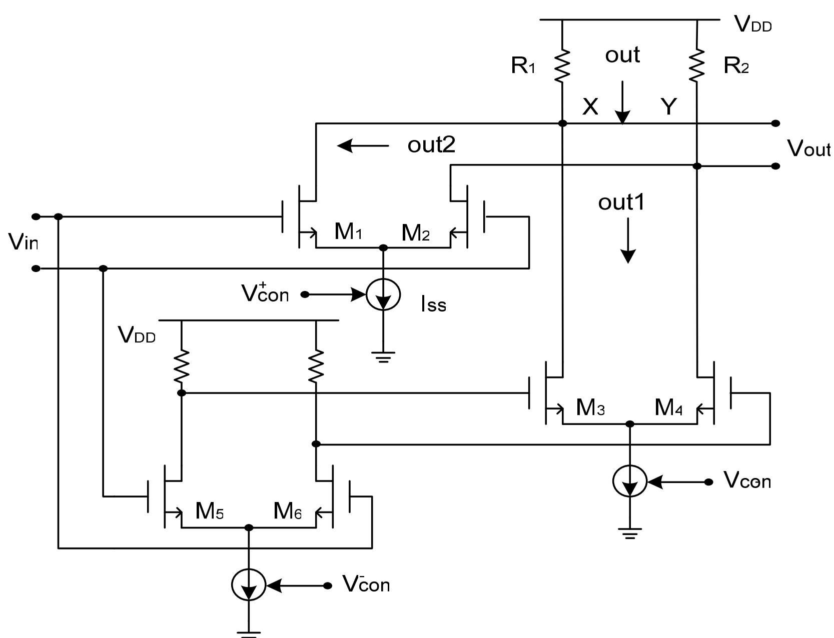

Figure 3.5 Interpolating delay stage

Illustrated in Figure 3.6, the resulting circuit employs the differential pair M_7-M_8 to steer Iss between M_1-M_2 and M_3-M_4. If V_{cont} is very negative, M_8 is off and only the fast path amplifies the input. Conversely, if V_{cont} is very positive, M_7 is off and only the slow path is enabled. Since the slow path in this case employs one more stage than the fast path, the interpolating delay stage achieves a tuning range of roughly two to one. For operation with low supply voltages, the control pair M_7-M_8 can be replaced by the current-folding topology [8].

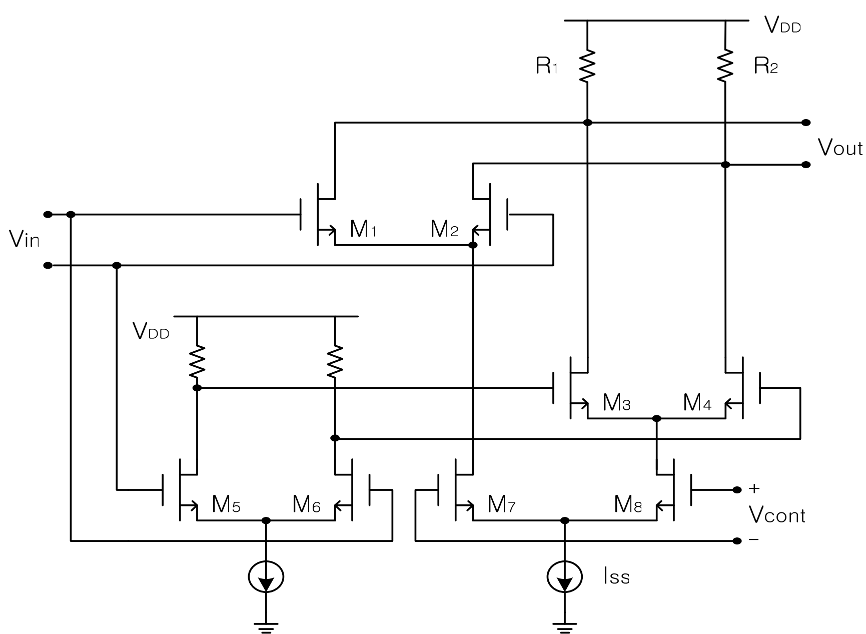

Figure 3.6 Interpolating delay stage with current steering

3.1.1.1 Interpolation Delay Cell Design

One delay cell consists of three differential buffer configurations, a voltage controller for slow or fast delay path selection, and a simple nMOS current mirror as shown in Figure 3.7. As a load transistor, instead of a pMOS transistor, an nMOS transistor was used because of its faster current flowing behavior.

Figure 2 The output waveform from XOR gate

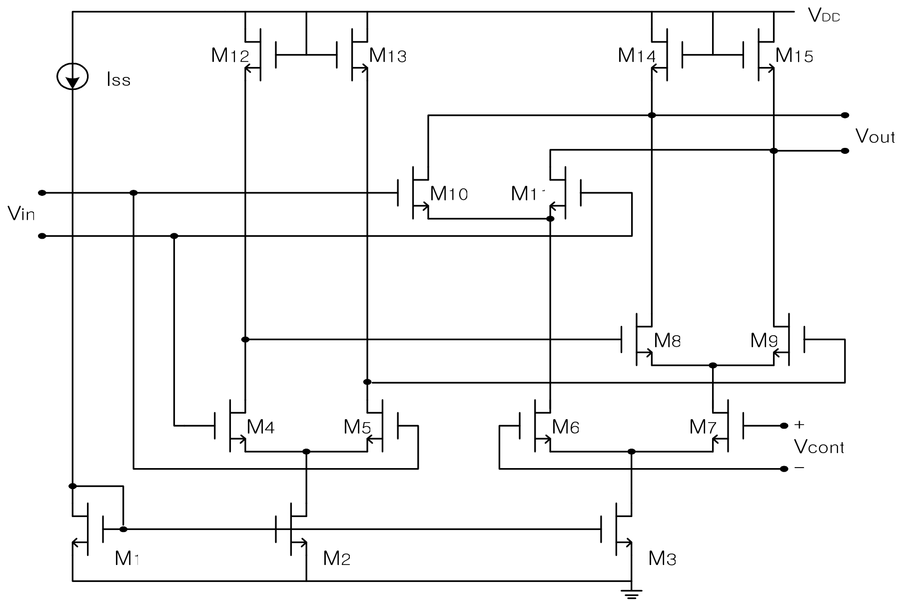

Figure 3.7 Interpolation delay cell for simulation

In this delay cell simulation, 1.8V DC power was supplied for Vdd, and the current source for the current mirror, Iss, was also selected as 400㎂ for this simulation. According to the value of current density in TSMC 0.18μ technology, 1㎃/㎛, the minimum channel length of MOSFETs should be at least 0.4㎛. The second consideration was the unity gain as a buffer/delay. In order to operate as a delay cell, it must not amplify the input signal, so, from the equation (3-2), M_4-M_{12}, and M_5-M_{13} have the same (W/L) sizes, and M_8-M_{14}, M_9-M_{15}, M_{10}-M_{14}, and M_{11}-M_{15} also have the same (W/L) sizes.

$$A_v \approx -\sqrt{\frac{\mu_n (W/L)_N}{\mu_n (W/L)_{N-load}}} \tag{3-2}$$

Then, the M_6, M_7 and M_1, M_2, and M_3 have been decided by considering logic depth and status of MOSFET operating modes, cut-off, linear, and saturation. This step is not very simple because it should be considered by related voltage values such as the input voltage range and voltage values at each transistor nodes.

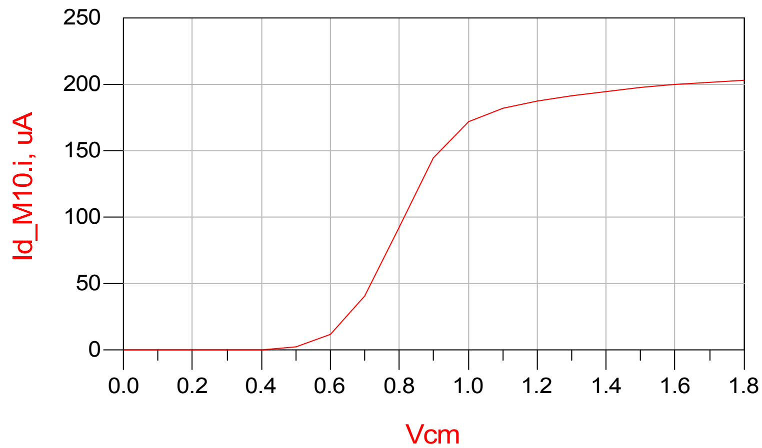

Figure 3.8 Common Mode Id-Vcm characteristics

From the Figure 3.8, the input range was selected between 0.45V to 1.4V, and the lowest input voltage has to be higher than VTH-N because the MOSFETs can work at least when their gate voltage is higher than their threshold voltages. So, the input voltage range for this circuit was decided initially from 600㎷ to 1.2V, which is on the linear region at Figure 3.8. Next, the widths of those transistors have to be large enough to handle the maximum current flowing, 400μA, and as mentioned earlier, they also have to be decided by the following saturation conditions, (3-3) and (3-4).

$$v_{GS} > V_T \,, \tag{3-3}$$

$$v_{DS} > v_{GS} - V_T \,. \tag{3-4}$$

However, because Vgs limits the transistor Id-Vds characteristic, which is a drain-current increasing limit, it means after reaching a certain width, increasing width is not effective to increase drain-current flowing. So, after optimization, the final values of (W/L) ratio are (3.4/0.4) for differential pairs, (66/0.4) for voltage controllable transistors, and (100/0.4) for current mirrors.

At last, the output current of the current mirror is an important factor to recognize the overall status of the circuit. The (W/L) ratios of current mirror transistors have to be the same to drive the same current values for output of 2 and 3, Figure 3.9, and also in Figure 3.5 and 3.6.

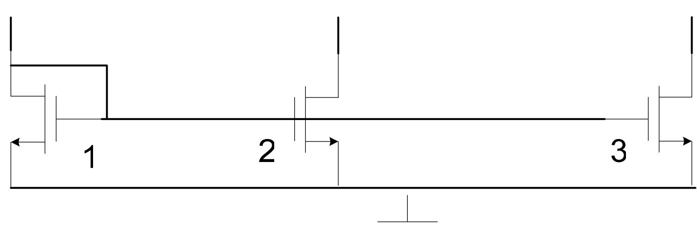

Figure 3.9 Current mirror with (W/L) ratios

$$I_{out} = \frac{(W/L)_2}{(W/L)_1} I_{REF} \tag{3-5}$$

$$I_{out} = \frac{1}{2}\mu_n C_{ox}\left(\frac{W}{L}\right)_{2,3}(V_{GS} - V_{TH})^2 \tag{3-6}$$

The V_{GS} on 1, 2, and 3 are the same as V_{d1} because the drain and gate are connected together, so the output currents of current mirrors are the same in (3-6).

In real simulation results, the current flow at the drain of the current mirror might not be the same as the reference value, I_{REF}, because of other operational transistors before the current mirrors. In this case, for the acceptable current mirror design, the differences of the current values of I_{REF} and I_{out} should be less than 10% of I_{REF}. So, lowest acceptable value of the current driving is 360㎂.

3.1.1.2 Folded Structure Design

The folded structure is basically for improving the input common-mode range and the power-supply rejection of the circuit. A simple differential pair is consisted of a current stage followed by a cascade current–mirror load. So the output is coming out from push-pull configuration.

In this thesis, the current control stage with V_{CONT} has been taken off from the non-folded schematic, and then pMOS cascade current mirror has been connected for controlling current flowing with pushing in current into the main differential pair instead of blocking current flowing. So there are two current mirrors existing on the folded delay schematic.

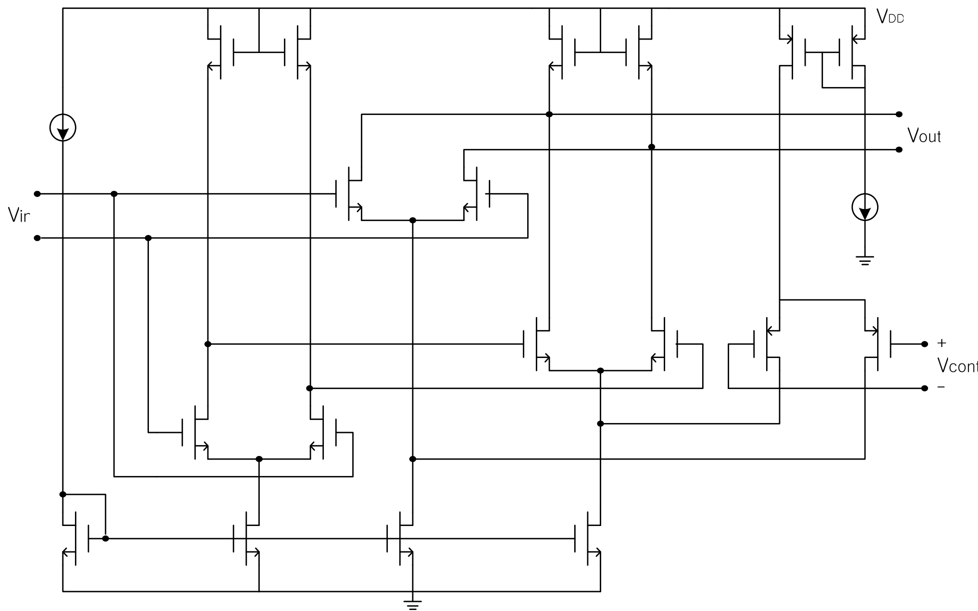

Figure 3.10 Schematic of folded interpolation delay cell

3.1.1.3 Simulation Result of Folded Delay Cell

In order to have wider input voltage range and output voltage swing, the folded structure is applied for this delay cell. The designed folded delay cell is simulated with the clock input signal of ΔV=600㎷, 0.7V~ 1.3V, and the input frequency range is the same as the previous simulation. The Figure 3.10 is the actual folded delay circuit schematic in ADS.

The Figure 3.11 is the output waves of the transient simulation on signal frequencies of 1GHz, 2GHz, and 3GHz. Input voltage range is from 0.7V to 1.3V.

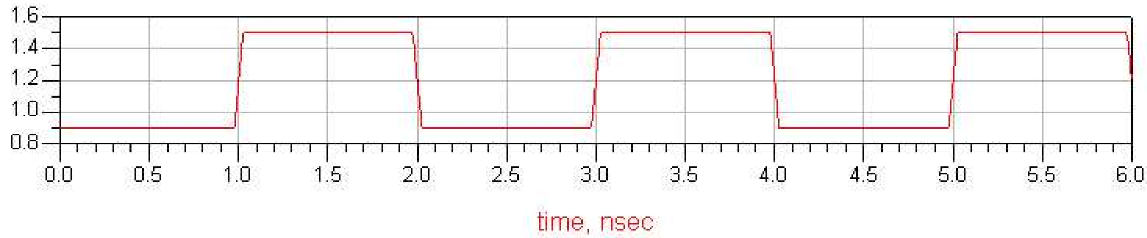

(a)

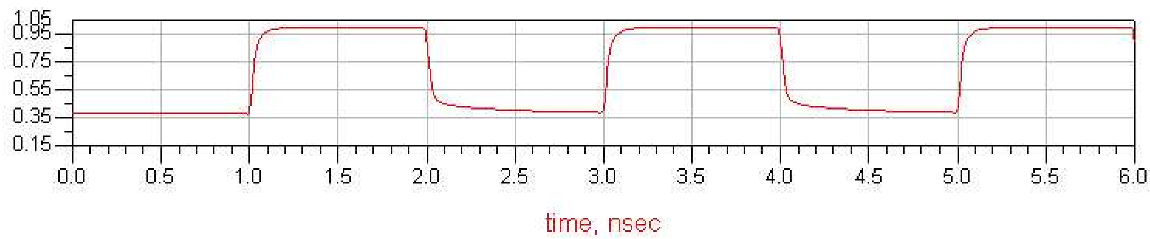

(b)

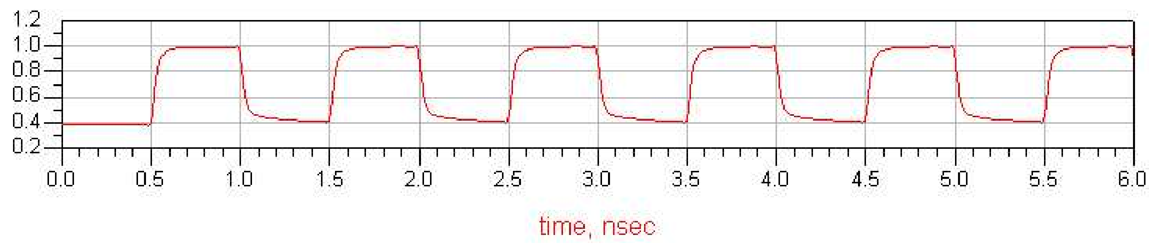

(c)

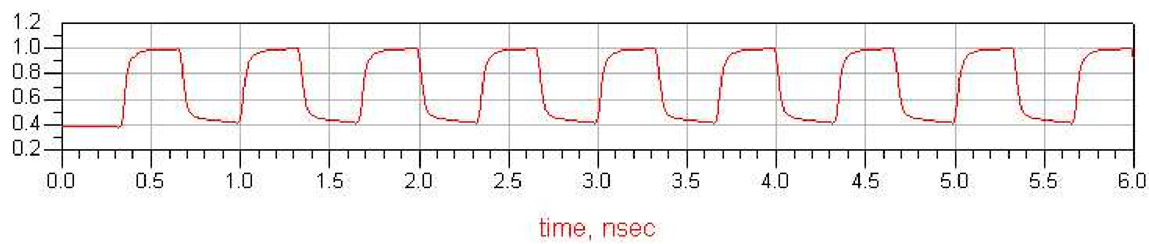

(d)

Figure 3.11 (a) 1GHz Input waveform (b) 1GHz Output waveform (c) 2GHz Output waveform, and (d) 3GHz Output waveform only fast path is working

This comparison table shows better voltage output swing of the folded delay cell simulation, Table 3-3.

Table 3.1 Output Voltage Swing of the Folded Case

Input frequency	Output voltage swing of folded case (㎷)	Differences, Δ (㎷)
1GHz	491.3	11.9
2GHz	462.2	12.6
3GHz	444.8	16.2

Next simulation results are the delayed output waves. The maximum delay time is 37ps, 4ps of propagation delay and 33ps of phase shifting delay time, in 1GHz input signal, Figure 3.12. The delay time is variable caused by voltage values of the V_{CONT}.

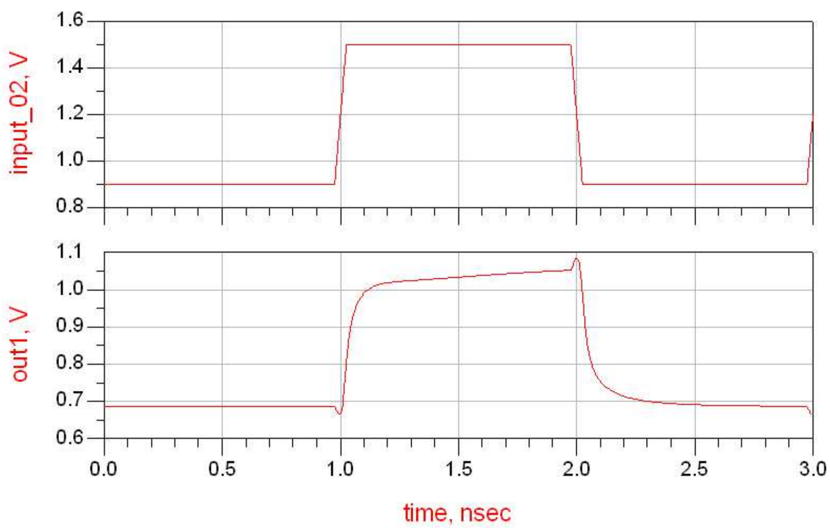

Figure 3.12 Maximum delay time

The total delay is the sum of propagation delay and shifted delay time (tp = 4ps and ts = 34ps. Total delay = 38ps, where input frequency is 1GHz)

Table 3.2 Maximum Delay Time by Different Input Frequencies

Input Frequency	Propagation Delay	Shifted Delay	Total Delay
1GHz	4ps	33ps	37ps
2GHz	2ps	34.3ps	36.3ps
3GHz	1ps	33.3ps	34.3

The following Table 3.3 and Figure 3.13 show the shifted delay time change caused by V_{CONT} change. For this thesis, an acceptable control voltage range is from 0.5V to 1.8V, Δ V = 1.3V. However, according to the delayed time increased, the useful voltage range is from 1.1V to 1.8V, Δ V = 0.7V.

Table 3.3 Shifting Time Changes by Variable V_{CONT} at 1GHz Input Frequency

V_{CONT} – fast (V)	V_{CONT} - slow (V)	Shifted Delay Time (ps)
1.5	0.5	1.3
1.4	0.6	2.3
1.3	0.7	3.3
1.2	0.8	4.3
1.1	0.9	3.3
1.0	1.0	3.3
0.9	1.1	3.3
0.8	1.2	6.3
0.7	1.3	25
0.6	1.4	28

Table 3.3 – continued

0.5	1.5	30
0.4	1.6	31
0.3	1.7	33
0.2	1.8	33

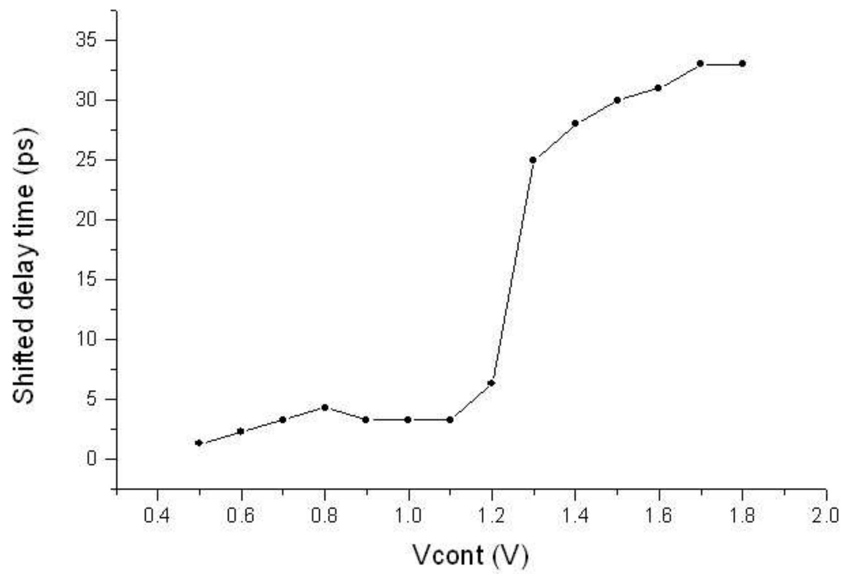

Figure 3.13 Shifted delay time change by Vcont change

3.1.1.4 Simulation Analysis and Result of Folded Delay Cell

On this delay-line, if it is compared with a single delay cell, the input clock voltages and current values are different, Figure 3.14. The 4 output of each between two cells were much slower than the single cell simulation because there is capacitance increasing by input MOS capacitance of the next cell, wires, and some parasitic capacitance.

$$t_{HL,LH} = \frac{C[V_{DD} - (V_{DD} - V_t)]}{\frac{1}{2}k'_n\left(\frac{W}{L}\right)(V_{DD} - V_t)^2} \tag{3-7}$$

According to the equation (3-7), the falling or rising time, t_{HL} or t_{LH}, is proportional to the total capacitance between the two cells. So, in order to increase or decrease the delay time, the width should be increased. However, if we increase the width of a transistor, also the capacitance will be increased. Finally, size increasing is not a solution, so increasing current could be one of the solutions, Figure 3.15.

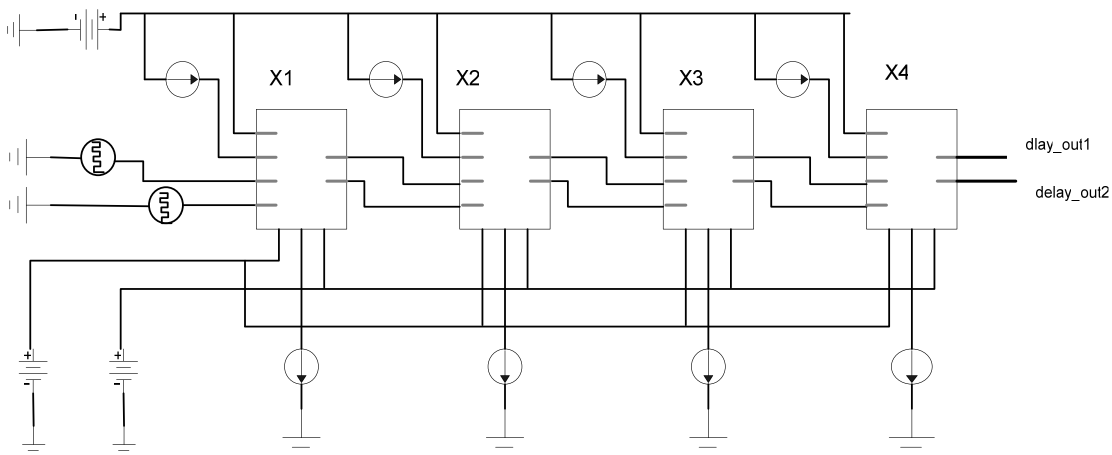

Figure 3.14 Test schematic of delay line

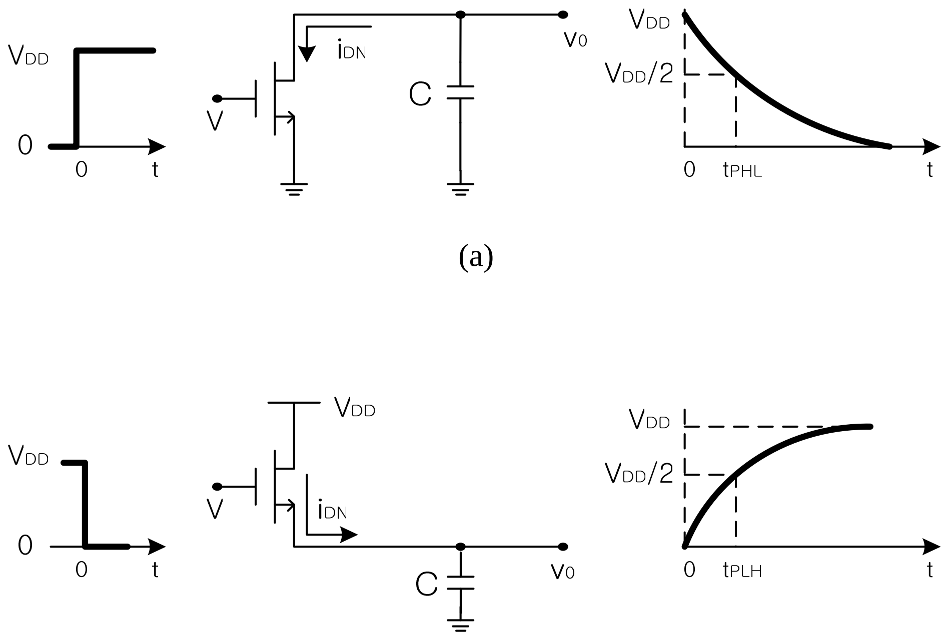

(a)

(b)

Figure 3.15 Equivalent circuits for determining the propagation delays (a) t_{PHL} and (b) t_{PLH} of the load side

$$i_{DN}(t) = k'_n \left(\frac{W}{L}\right)_n \left[(V_{DD} - V_t)\frac{V_{DD}}{2} - \frac{1}{2}\left(\frac{V_{DD}}{2}\right)^2 \right] \tag{3-8}$$

$$t_{HL,LH} = \frac{C\Delta V}{i_{DN}} = \frac{CV_{DD}/2}{i_{DN}} \tag{3-9}$$

Figure 3.16 shows output waves after each delay cells. We can see the delay time with shifted waves. The input signal was 1GHz clock waves.

Delay time exits not only in each delay block, but also between each gate.

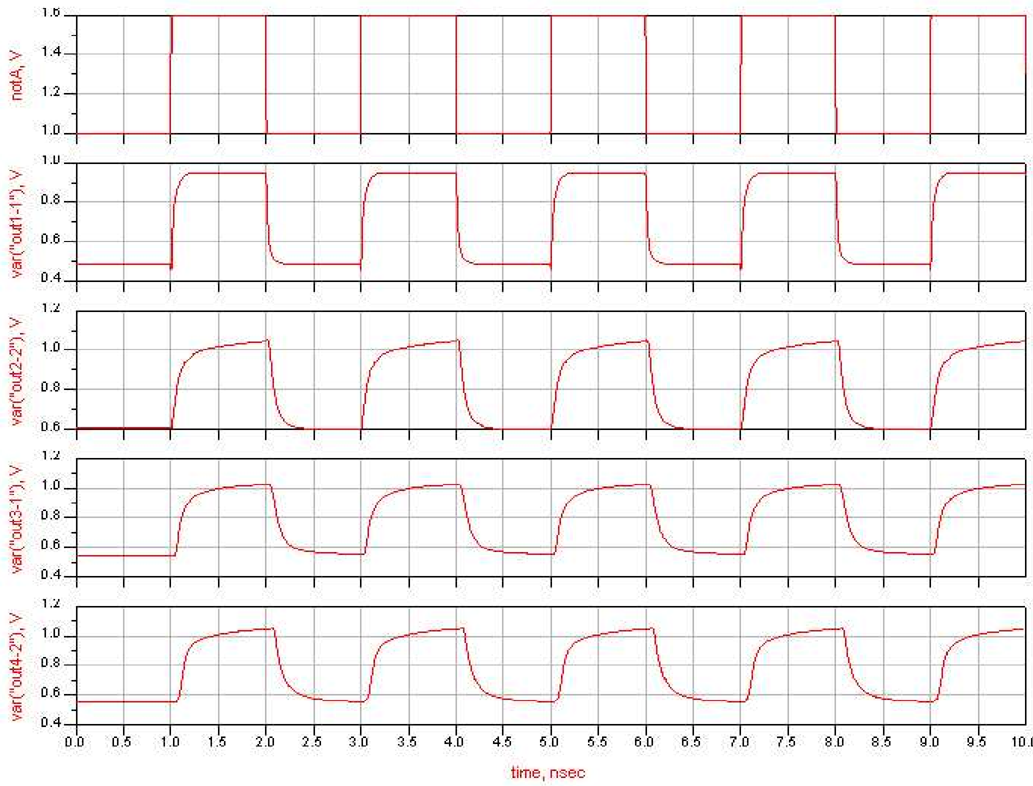

Figure 3.16 1GHz input clock signal and output waves at each cell of a delay line

3.1.2 Gilbert Cell Structure (XOR)

Analysis a differential pair, the small-signal gain variation as a function of the tail current. The current steering on each output node caused by load resistors is one of the most important points to analyze the simple differential pair. So, there is a combined differential pair of which the gain can be controlled by a voltage, Figure 3.17.

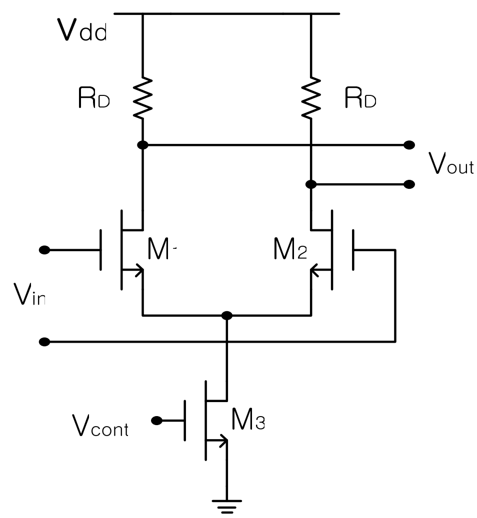

Figure 3.17 Variable Gain Amplifier (VGA)

The control voltage decides the tail current and then the gain of the differential pair. In this topology, $A_V = V_{out} / V_{in}$ varies from zero (if I_{D3}=0) to a maximum value given by voltage headroom limitations and device dimensions. This circuit is a simple example of a "variable-gain amplifier" (VGA). When the signal amplitude has a large variation, VGA can be applied in systems to minimize the variation of the gain [8].

Now, suppose the amplifier's gain can be continuously varied from a negative value to a positive value. Consider two differential pairs that amplify the input by opposite gains, Figure 3.18. We now have $V_{out1} / V_{in} = - g_m R_D$ and $V_{out2} / V_{in} = + g_m R_D$, where g_m denotes the transconductance of each transistor in equilibrium. If I_1 and I_2 vary in opposite directions, so do $| V_{out1} / V_{in} |$ and $| V_{out2} / V_{in} |$ [8].

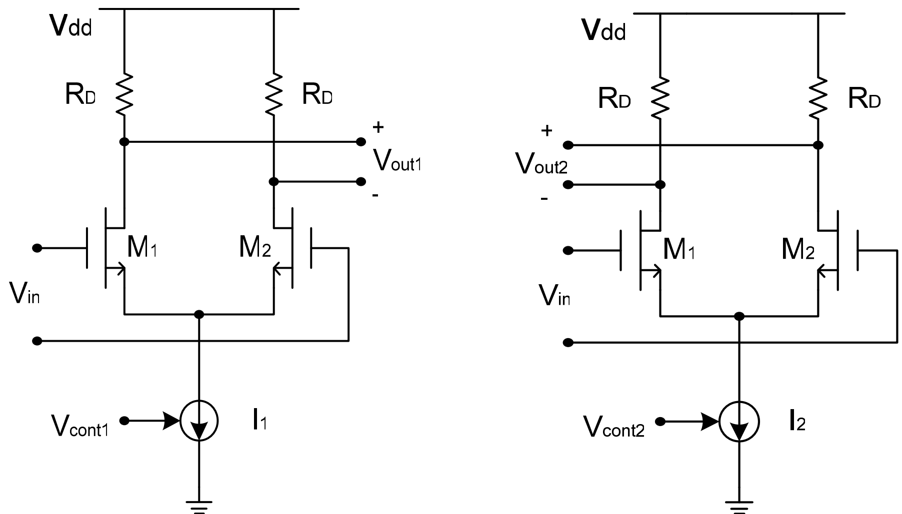

Figure 3.18 Two stages providing variable gain

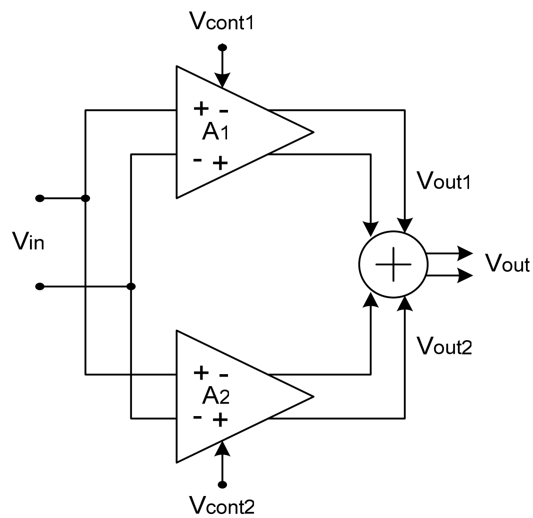

Figure 3.19 Summation of the output voltages of two amplifiers

The Figure 3.20 shows summation of the two output voltages from each VGA amplifiers. The final output voltage must be proportional of each gain, which is controlled by V_{cont} at its amplifier.

$$V_{out} = (A_1 + A_2)V_{in} \tag{3-10}$$

$$V_{out1} = A_1 V_{in} = R_D I_{D1} - R_D I_{D2} \tag{3-11}$$

$$V_{out2} = A_2 V_{in} = R_D I_{D4} - R_D I_{D3} \tag{3-12}$$

Rather than add V_{out1} and V_{out2}, we simply short the corresponding drain terminals to sum the currents and subsequently generate the output voltage, Figure 3.18. Note that if I_1=0, then $V_{out} = + g_m R_D V_{in}$ and if I_2=0, then $V_{out} = - g_m R_D V_{in}$. For $I_1 = I_2$, the gain drops to zero [8].

On this combination of two differential pair, the currents controlled by V_{cont} will have opposite directions, and definitely, the gains can be changed by the current. The steered currents and gain on each sided amplifier are following the values of V_{out1} and V_{out2}, and when the two voltages are the same, the gain of the amplifier will be zero. This circuit, Figure 3.21, is generally called a "Gilbert cell" [24], which is the most popular circuitry for Analog and RF communication area. Also, it is very popular for building MUX and XOR.

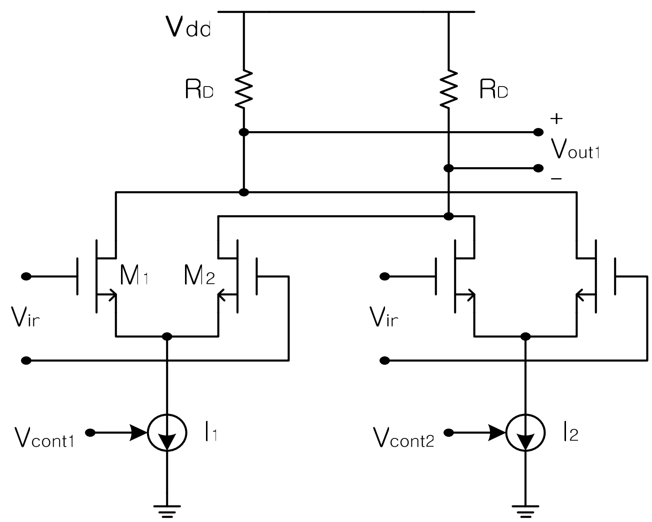

Figure 3.20 Summation in the current domain

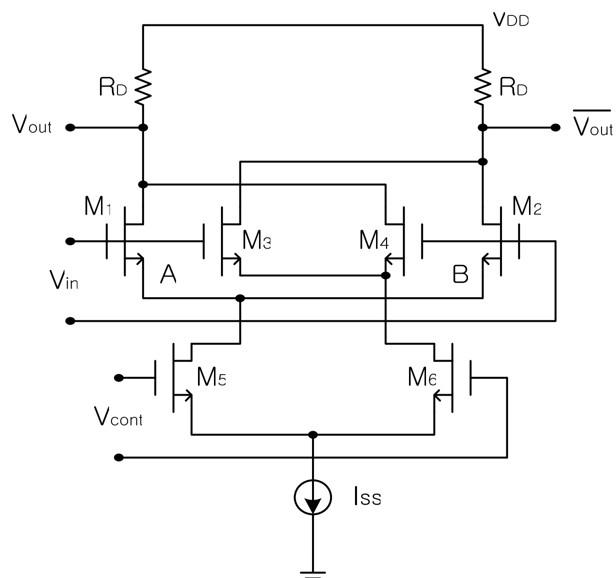

Figure 3.21 Gilbert cell

As with a cascade structure, the Gilbert cell consumes greater voltage headroom than a simple differential pair. This is because the two differential pairs M_1-M_2 and M_3-M_4 are “stacked” on top of the control differential pair, Figure 3.22. To understand this point, suppose the differential input, V_{in} has a common-mode level $V_{CM,in}$. Then $V_A = V_B = V_{CM,in} - V_{GS1}$, where M_1- M_4 is assumed identical. For M_5 and M_6 to operate in saturation, the CM level of V_{cont}, $V_{CM,COM}$ must be such that $V_{CM,COM} \leq V_{CM,in} - V_{GS1} + V_{TH5,6}$. Since $V_{GS1} - V_{TH5,6}$ is roughly equal to one overdrive voltage, we conclude that the control CM level must be lower that the input CM level by at least this value.

The Gilbert cell topology is showing in Figure 3.22 (a). We choose to vary the gain of each differential pair through its tail current thereby applying the control voltage to the bottom pairs and the input signal to the top pairs. Interestingly, the order can be exchanged while still obtaining a VGA. The idea is to convert the input voltage to current by means of M_5 and M_6 and route the current through M_1-M_4 to the output nodes. If V_{cont} is very positive, then only M_1 and M_2 are on and $V_{out}=g_{m5,6}R_DV_{in}$. Similarly, if V_{cont} is very negative, then only M_3 and M_4 are on and $V_{out}=-g_{m5,6}R_DV_{in}$. If the differential control voltage is zero, then V_{out} =0. The input differential pair may incorporate degeneration to provide a linear voltage-to-current conversion [8].

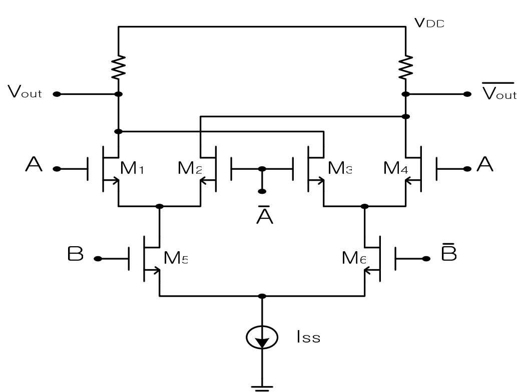

(a)

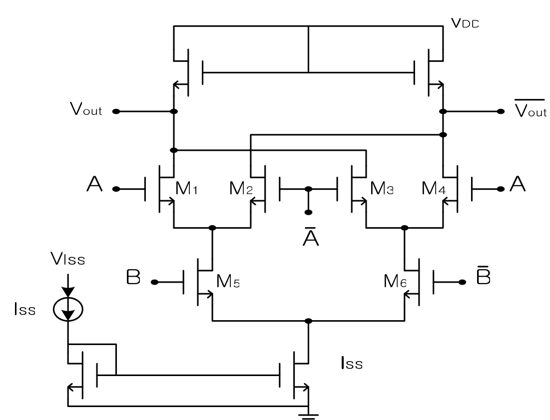

(b)

Figure 3.22 Gilbert cell with (a) passive and (b) nMOS load

A CML XOR is shown in Figure 3.22 (b). To achieve high-speed performance, their transistors work in a linear region and can be represented with a linear model identical for the circuit [23].

3.1.2.1 Design for XOR Gate

This Gilbert cell is very famous circuitry in RF, and it is being used as a standardized structure, so in this thesis, the Gilbert cell has been applied for XOR directly. Also, on this Gilbert cell, all passive components have been replaced by all active components. The XOR has two different levels of input signals. Each input voltage values can be decided by DC common mode simulation, Figure 3.23, so the decided input voltage ranges are,

Input A voltage range: 1V~1.6V

Input B voltage range: 0.7V~1.3V

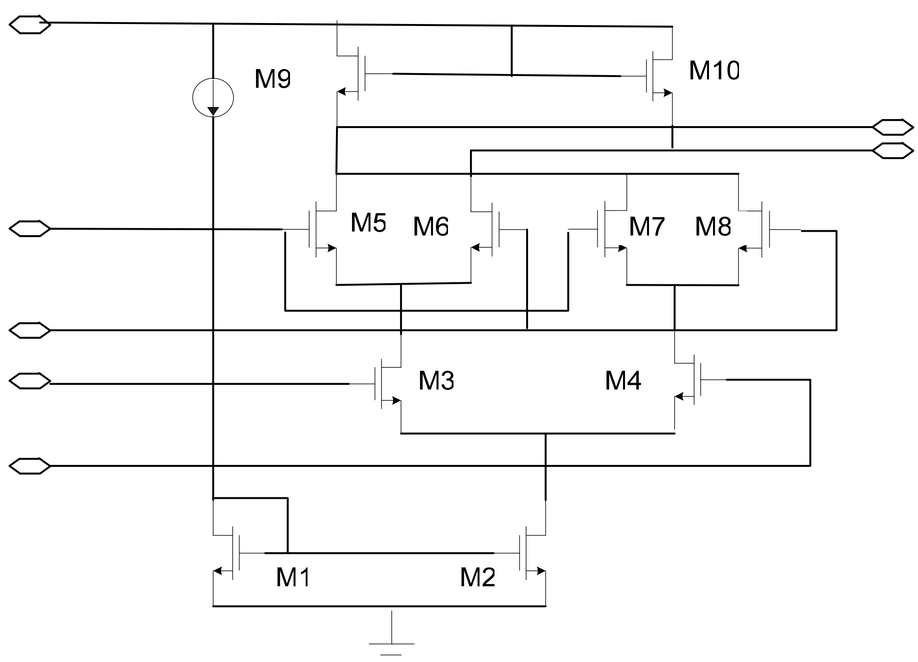

Figure 3.23 Schematic of XOR DC common mode simulation

The XOR cell, working for phase detection, was simulated with two different signals. One is on upper level which stands for the delay-line and the other is in lower level, the original signal, the same as the input signal into the delay cell. The upper level signal was ΔV=600㎷, 0.7V~1.3V, of a clock signal, and the lower level signal was also ΔV=600㎷. However, the input voltage swing range was lower than the upper signal because the voltage across the lower level input transistors are smaller than the upper case. The voltage would be dropped before reaching the lower input transistors by other upper transistors, thus the swing range, 0.6V~1.2V, was selected. Also the input clock frequency is 1GHz, which is mentioned before, for optical Ethernet application, and general UWB operating frequencies.

Then, the output waves of the transient simulation on signal frequencies of 1GHz are the following Figure 3.24. The random bits signal was put into the circuit, so the XOR would detect different input level of two input levels, and then it made a short pulse on each output node.

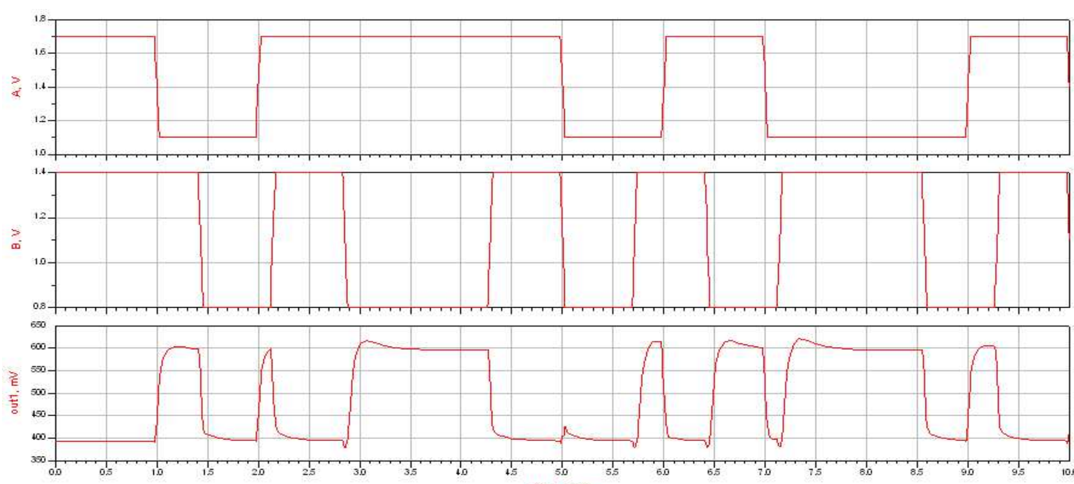

Figure 3.24 1GHz input random and different frequency signal, and output wave

3.1.2.2 Simulation Result of XOR Gate

Next, at the end of the delay line, the XOR cell was connected. Figure 3.25 is the schematic of the pulse generator on ADS. From the one-pair input signal source, upper level input and lower level input are providing at the same time. Of course, they are from the output of the delay line. This circuit detects different phase of the two signals. Whenever it has been detected, a pulse will be generated. The pulse width is the same as delay time. As describing before, the pulse will be generated by the XOR cell. After the XOR gate, the pulse is detected. The output waveform is shown below.

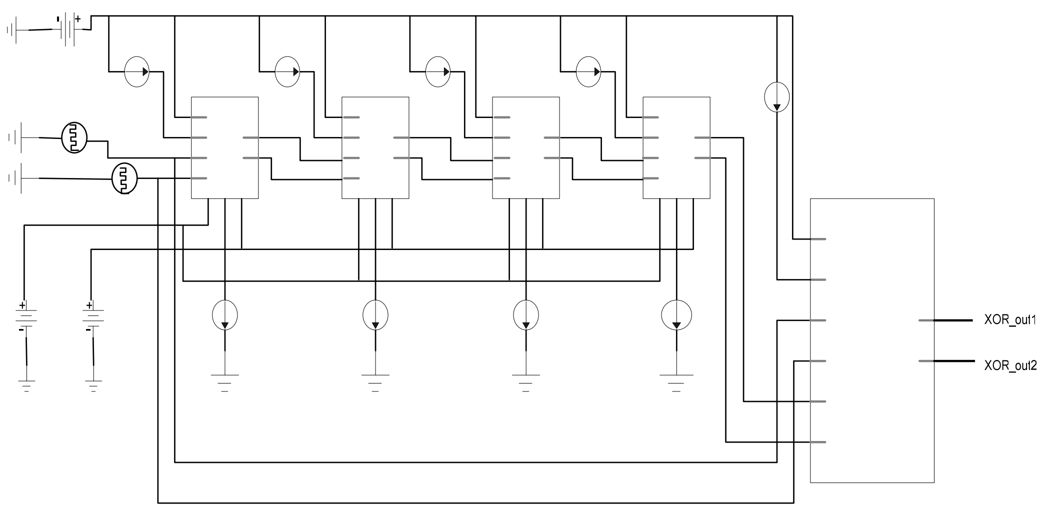

Figure 3.25 Test schematic of the pulse generator

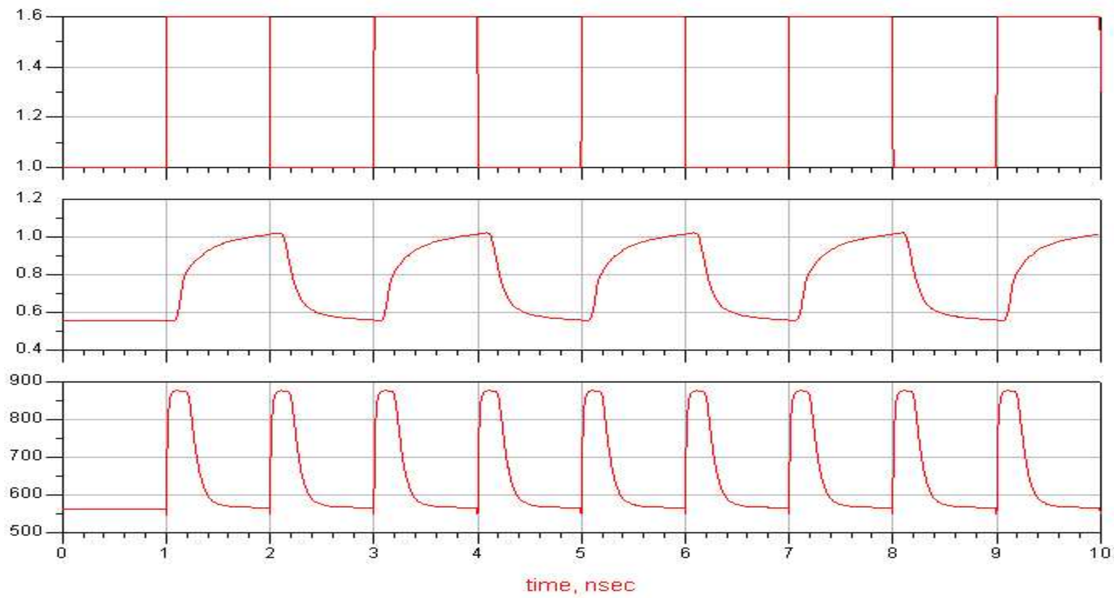

Figure 3.26 1GHz input clock and the last output waveform the delay cell and the XOR gate of a pulse generator

3.2 Impulse Shaping Circuit (FIR filter)

According to the UWB communication block diagram in this thesis, after square shape pulses are made, the impulse shaping step is required to generate a base impulse signal for modulation, which is one of Gaussian pulse families, Figure 3.27.

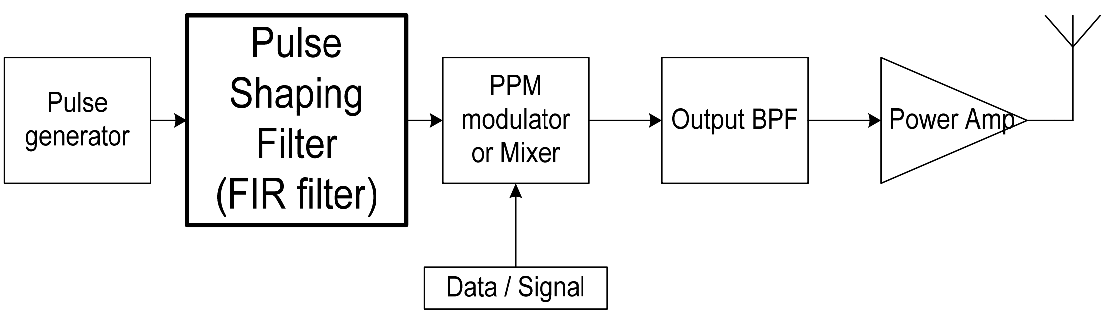

Figure 3.27 Block diagram for pulse shaping filter

The generated pulse shape is really dependant on the pulse shaping filter. In this case, also generally, a Band-Pass Filter, BPF, is applicable for the pulse shaping circuit. The pulse after this BPF will be the same shape as Gaussian pulse families.

Gaussian pulse has better power performance than the other waves; also derive the pulse to yield waveforms with an additional zero crossing. Each different Gaussian pulses have different power spectrum, as mentioned in chapter 2. So for the UWB wireless communication system, over 3.1GHz range, and FCC power limitation, thus the Gaussian pulse has been considered. Additionally, Gaussian pulse can be shaped easily compared with others. That is the reason of using a Gaussian pulse in time domain for UWB technology.

As mentioned in chapter 2, the power spectrum density of generated Gaussian impulse by previous impulse generator can not meet the FCC regulation. According to the simulation in Matlab, the PSD of 5^{th} derivative Gaussian pulse meets the FCC regulation. And the same time, the RCL shaping circuit occupies a huge area in the chip. Implementing the active components as the filter as the pulse shaper is the best choice.

FIR filter, as the pulse shaper, shapes the Gaussian monopulse which comes out from XOR gate. The operation of the FIR filter is convolving the input signal with the impulse response to shape the pulse. The 5^{th} derivative Gaussian is generated from FIR filter for UWB communication.

The 5^{th} derivative Gaussian satisfies the FCC emission limits for UWB systems. It also maximizes the bandwidth. By increasing the occupied bandwidth of the pulse, the overall data rate and the distance can be increased. This factor is what allows UWB systems to operate at a very low average transmit PSD, while achieving useful data rates and transmission ranges [25].

Next chapter will introduce the FIR filter and how it generates the 5th Gaussian pulse.

3.3 Gaussian Monopulse Generator

The original design for pulse shaping circuit is RLC Resonant Band-Pass filter. The Gaussian pulse is generated by the XOR gate and then shaped by RLC BPF. The 1st derivative Gaussian pulse is generated (Figure 3.28). By exporting the data from ADS to Matlab and simulating in Matlab, the PSD of the 1st Gaussian can not meet the FCC regulation as showing in Figure 3.30. Although the passive BPFs can shape the pulse to meet the FCC regulation by adding more LC ladder network, the passive components occupy huge area than the active components. Those reasons lead us to design the filter which is composed of the active components

Our previous impulse shaper using the BPF circuit is a simple LC parallel filter.

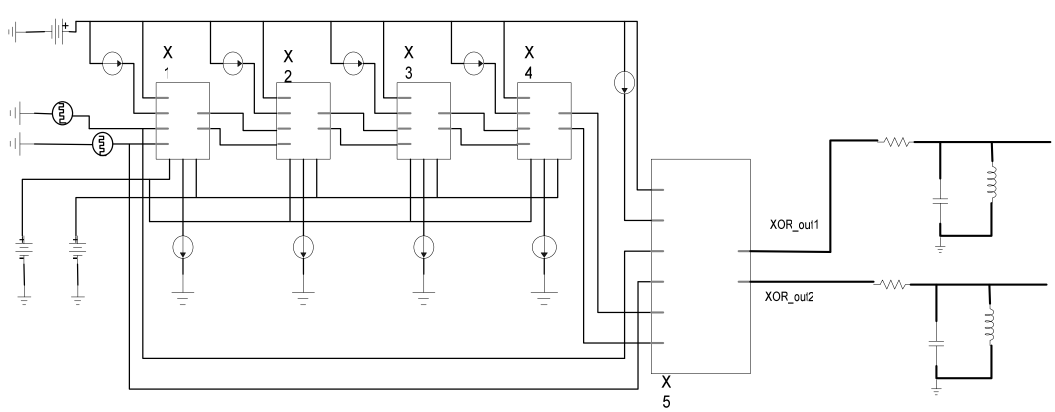

Figure 3.28 Test schematic of the pulse generator with BPF.

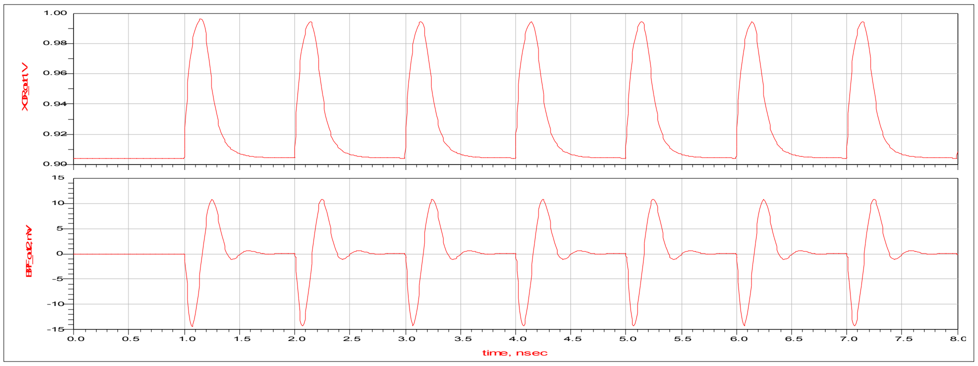

Figure 3.29 The generated output waves and shaped impulses after passing the XOR and BPF.

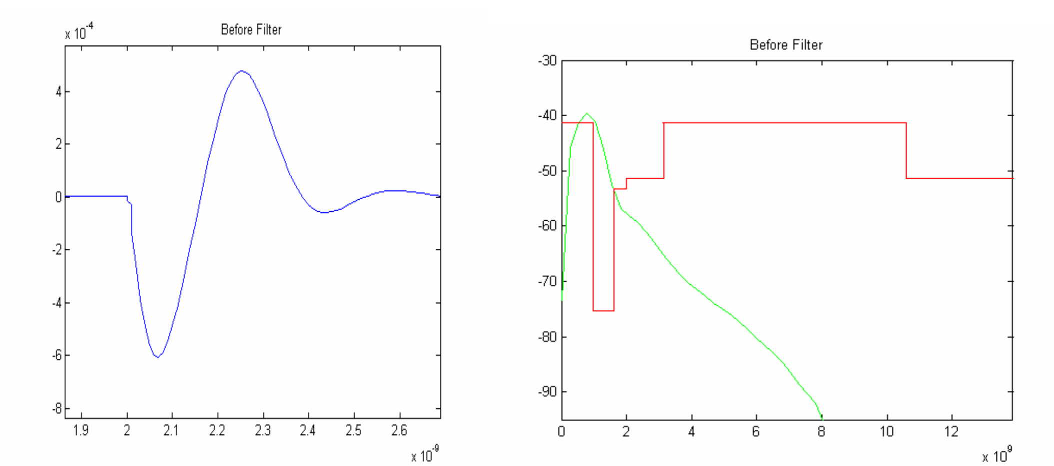

(a). (b).

Figure 3.30 (a) The 1st derivative Gaussian pulse from BPF and (b) its PSD

CHAPTER 4

FINITE IMPULSE RESPONSE (FIR) FLTER – PULSE SHAPER

Filters are an important issue of linear time-invariant systems. The term frequency-selective filter proposes a system that passes certain frequency components and completely rejects all others. In a general context, any system that modified certain frequencies relative to other is also called filter [10].

The following stages describe how to design the filter: (1) the requirement of the desired properties of the system, (2) the approximation of the specifications using causal discrete-time system, and (3) the understanding of the system [10].

In a realistic setting, the desired filter is generally implemented with digital calculation and used to filter a signal that is derived from a continuous-time signal [10].

4.1 FIR Filter as the Pulse Shaper

Shaping the spectrum by changing the pulse waveform is an interesting characteristic of impulse radio. Basically, the spectrum could be shaped in pulse width variation, pulse differentiation, and combination of base functions. FIR filter, as the pulse shaper, shapes the spectrum of the Gaussian monopulse for UWB communication application. Since shaping the pulse also affects the power spectrum density of the transmitted signal, the choice the impulse response of the FIR filter is very important. FIR filter also acts as a differentiator to derive the Gaussian monopulse. Differentiation of the Gaussian pulse influences the energy spectrum density. The peak frequency and bandwidth of the pulse are also different while increasing the differentiation order. The following equation shows that Gaussian derivatives of higher order are characterized by higher peak frequencies. Differentiation is the way to move energy to higher frequency bands [17].

$$f_{peak,k} = \sqrt{k}\,\frac{1}{\alpha\sqrt{\pi}} \tag{4.1}$$

f_{peak}: peak frequency; k: the order of differentiation;α: shape factor.

The proposed FIR filter will differentiate the Gaussian monopulse to generate the 5th derivative Gaussian pulse. In the following sections will introduce the FIR filter's theory and characteristics and how to design the FIR filter as the pulse shaper [17].

4.2 The Theory and Characteristics of the FIR Filter

4.2.1 The Theory of the FIR Filter

A finite impulse response (FIR) filter has a finite impulse response. The system of the impulse response is a finite sum:

$$h[t] = a_0\delta[t - T_d] + \cdots + a_m\delta[t - mT_d] \tag{4.2}$$

FIR filters perform a convolution of the filter coefficients with a sequence of input signals and produce an equally numbered sequence of output signals (equation4.3). The convolution constructs the response of a linear system to an arbitrary input signal as a sum over suitably delay and scaled impulse response.

$$y(t) = x(t) \otimes h(t) \tag{4.3}$$

The FIR filtering in time domain uses convolution process.

1st, the input signal can be decomposed into a set of impulses, each of which can be viewed as a scaled and shifted delta function.

2nd, the output resulting from each impulse is a scaled and shifted version of the impulse response.

3rd, the overall output signal can be found by adding these scaled and shifted impulse responses.

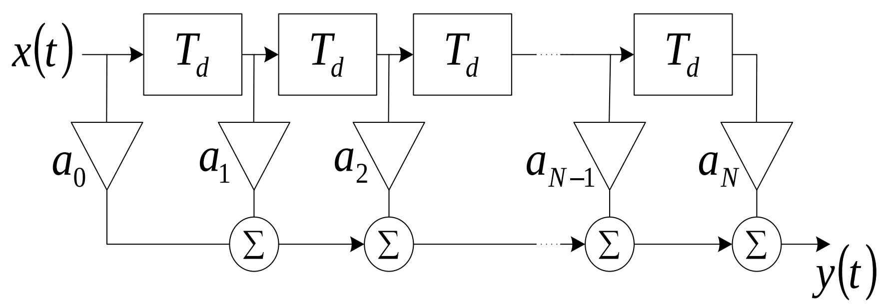

Figure 4.1 The structure of the FIR filter

$x(t)$: input to FIR filter

T_d : the time delay between taps in the filter

a_k : the amplifier coefficients

$y(t)$: output of the FIR filter

The FIR filter includes two main parts: delay element and multiplier.

1. Delay element:

Analog delay: y_T=x (t-T), y_T equals the input x (t) delay; $y_T(s)=e^{-sT}X(s)$;

$$x(t) \longrightarrow \boxed{T_d} \longrightarrow y_T(t)=x(t-T)$$

Figure 4.2 The delay block of the FIR filter (in time domain)

In the Z domain: y[n] =x [n-1], y[n] equals the input x[n] delay; y[n]=z^{-1}*x[z];

$$x[n] \longrightarrow \boxed{Z^{-1}} \longrightarrow y[n]=x[n-1]$$

Figure 4.3 The delay block of the FIR filter (in z domain)

It shows that the system function of the delay element is an exponential.

$$H_T(s) = e^{-sT} \tag{4.4}$$

and its impulse response a delay impulse

$$h(t) = \delta(t-T) \tag{4.5}$$

The structure of our FIR filter consists of delay blocks and a set of coefficients. The structure of our FIR filter is shown in Fig.4.1. When the impulse response of a system is known, the complete characteristics of the system are known, too. The reaction of the system to any other input can be determined by using convolution. The output of the system is determined by computing a sum of products of the impulse response coefficients α_k and past value x (t-kT_d). From a practical standpoint, the simpler function is typically specified in the time-shift format.

$$y(t) = \sum_{k=0}^{N} a_k x(t - kT_d) \tag{4.6}$$

4.2.2 Characteristics of the FIR Filter

There are some characters to describe the FIR filter: impulse response, frequency response, and phase response.

1. Impulse response:

Impulse response for LTI system entirely characterizes the system. Since the impulse response convolves with the input signal, it tells you everything about the system. The “impulse response” of a FIR filter is actually just the set of FIR coefficients. FIR filter has finite impulse response because there is no feedback in the filter.

2. Phase Response:

FIR filter always linear phase means the phase response of the filter is a linear (straight – line) function of the frequency. This result in the delay through the filter is the same at all frequencies. Therefore the filter does not cause “phase distortion” or “delay distortion”. FIR filters are usually designed to be linear-phase. A FIR filter is linear-phase if its coefficients are symmetrical around the center coefficient that is the first coefficient is the same as the last.

3. Frequency Response:

The frequency response of a linear time-invariant system is the Fourier transform of the impulse. The frequency response of a filter consists of its magnitude and phase responses. The magnitude response indicates the ratio of output amplitude to its input amplitude.

Simple filters are usually defined by their responses to the individual frequency components that constitute the input signal. There are three different types of responses. A filter's response to different frequencies is characterized as passband, transition band or stopband. The passband response is the filter's effect on frequency components that are pass through unchanged. Frequencies within a filter's stopband are highly attenuated. The transition band represents frequencies in the middle, which may receive some attenuation but are not removed completely from the output.

4.3 The Design and Implementation of the FIR Filter

The interesting part of designing FIR filter is translating the desired frequency response into filter tap coefficients. The process of selecting the filter's tap numbers and coefficients is called filter design. As can be seen from Figure 4.1, the equation for the output of an FIR in time domain is

$$y(t) = \sum_{k=0}^{n} h[k]\, x\left(t - \frac{k}{f_s}\right) \tag{4.7}$$

f_s: the sampling frequency; k: the filter tap number.

Since a delay of 1 / f_s in time corresponds to a multiplication by a complex exponential, the corresponding equation in the frequency domain is:

$$Y(f) = H(f)X(f) \tag{4.8}$$

$H(f) = \sum_{k=0}^{n} h[k] e^{-j2\pi \frac{f_k}{f_s}}$ is the frequency response of the FIR filter. (4.9)

$h[k] = \frac{1}{f_s} \int_0^{f_s} H(f) e^{j2\pi \frac{f_k}{f_s}} df$: the tap coefficients (4.10)

For designing the FIR filter, the desired frequency response, H (f), should be decided and then calculate the tap coefficients. But the actual frequency response will only approximate the desires response because the number of filter taps is finite.

The Parks-McClellan algorithm is the most widely used FIR filter design method. It is an iteration algorithm that accepts filter specifications in terms of passband and stopband frequencies, passband ripple, and stopband attenuation. The Parks-McClellan algorithm will be introduced in the next section [10].

4.3.1 Parks-McClellan Algorithm

For designing the impulse response of the FIR filter, the *firpm* function can be used in Matlab. The *firpm* function implements the Parks-McClellan algorithm, which uses the Remez Exchange algorithm and Chebyshev approximation theory. The Parks-McClellan algorithm optimizes frequency responses by minimizing the maximum error (equation 4-11) between the desired frequency response and the actual frequency response (equation4-12) [10]. They are sometimes called minimax filters.

$$\delta_{\min i \max} = \min\{\max(E(\omega))\}; \tag{4-11}$$

$$A_e\left(e^{j\omega}\right) = h_e[0] + \sum_{n=1}^{L} 2h_e[n]\cos(\omega n) \tag{4-12}$$

$$E(\omega) = W(\omega)\left[H_d\left(e^{j\omega}\right) - A_e\left(e^{j\omega}\right)\right] \tag{4-13}$$

W(ω): weighting function; incorporates the approximation error parameters into design process.

$H_d(e^{j\omega})$: desired frequency response;

$A_e(e^{j\omega})$: actual frequency response. $\cos(\omega n) = T_n(\cos\omega)$

The Park-McClellan algorithm is according to reformulating the filter design problem while a problem in polynomial approximation. Specially, the terms cos(ωn) in (4-12) can be expressed as a sum of powers of cos(ω) in the form cos(ωn) = T_n (cos ω), where $T_n(x)$ is an nth-order polynomial. Consequently, equation (4-12) cab be written as an Lth-order polynomial in cosω,

$$A_e\left(e^{j\omega}\right)=\sum_{k=0}^{L} a_k\left(\cos\omega\right)^k \tag{4-14}$$

where the α_k's are constants that are related to $h_e[n]$, the values of the impulse response. With the substitution x= cosω, we can express $A_e(e^{j\omega})=P(x)\big|_{x=\cos\omega}$, where P(x) is the Lth-order polynomial

$$P(x)=\sum_{k=0}^{L} a_k x^k \tag{4-15}$$

[10].

The key to gaining control over ω_p and ω_s is to fix them at their desired values and let $\delta_1$and δ_2 differ. Parks and McClellan showed that with L, ω_p and ω_s fixed, then the frequency-selective filter design problem becomes a problem in Chebyshev approximation over disjoin set. To formalize the approximation problem, an approximation error function (4-13)[10].

The particular criterion used in this design procedure is the minimax or Chebyshev criterion. Within the frequency intervals, we look for a frequency response $A_e(e^{j\omega})$ that minimizes the maximum weighted approximation error of equation (4-13). The best approximation is to be found in the logic of

$$\min_{\{h_e[n]\,0\le n\le L\}} \left(\max_{\omega\in F} |E(\omega)| \right) \tag{4-16}$$

F is the closed subset of $0\le\omega\le\pi$, such that $0\le\omega\le\omega_p$ or $\omega_s\le\omega\le\pi$. Thus, we search for the set of impulse response values that minimize the δ.

Parks and McClellan applied the Alternation Theorem of approximation theory to this filter design problem.

4.3.1.1 Alternation Theorem

Alternation Theorem Let F_p denote the closed subset consisting of the disjoint union of closed subsets of the real axis x. Then

$$P(x) = \sum_{k=0}^{r} a_k x^k \tag{4-17}$$

is an rth-order polynomial. Also, $D_p(x)$ denotes a given desired function of x that is continuous on F_p ; ω_p (x) is a positive function, continuous on F_p, and

$$E_p(x) = W_p(x)[D_p(x) - P(x)] \tag{4-18}$$

is the weighted error. The maximum error is defined as

$$\|E(x)\| = \max_{x\in F_p} |E_p(x)| \tag{4-19}$$

A necessary and sufficient condition that P(x) is the unique rth-order polynomial that minimize $|E(x)|$ is that $E_p(x)$ exhibit at least (r+2) alternations; i.e. there must exist at least (r+2) values x_i in F_p such that $x_1 < x_2 < \ldots x_{r+2}$ and such that

$$E_p(x_i) = -E_p(x_{i+1}) = \pm\|E\| \text{ for } i = 1,2,\cdots,(r+1). \tag{4-20}$$

The alternations theorem provides necessary and sufficient conditions on the error for optimality in the Chebyshev or minimax logic.

From the alternation theorem, we know that the optimum filter $A_e(e^{j\omega})$ will satisfy the set of equations

$$W(\omega_i)\left[H_d\left(e^{j\omega}\right)-A_e\left(e^{j\omega}\right)\right]=(-1)^{i+1}\delta\,,\ i=1,2,\cdots,(L+2), \tag{4-21}$$

δ is the optimum error and $A_e(e^{j\omega})$ is given by equation (4-12) or (4-14). Using (4-14), for $A_e(e^{j\omega})$, we can write the equations

$$\begin{bmatrix} 1 & x_1 & x_1^2 & \cdots & x_1^L & \frac{1}{W(\omega_1)} \\ 1 & x_2 & x_2^2 & \cdots & x_2^L & \frac{-1}{W(\omega_2)} \\ \vdots & \vdots & \vdots & \cdots & \vdots & \vdots \\ 1 & x_{L+2} & x_{L+2}^2 & \cdots & x_{L+2}^L & \frac{(-1)^{L+2}}{W(\omega_{L+2})} \end{bmatrix} \begin{bmatrix} a_0 \\ a_1 \\ \vdots \\ \delta \end{bmatrix} = \begin{bmatrix} H_d\left(e^{j\omega_1}\right) \\ H_d\left(e^{j\omega_2}\right) \\ \vdots \\ H_d\left(e^{j\omega_{L+2}}\right) \end{bmatrix} \tag{4.22}$$

where $x_i = \cos\omega_i$. This set of equations serves as the basis for an iterative algorithm for finding the optimum $A_e(e^{j\omega})$. The procedure begins by guessing a set of alternation frequency ω_i fori=1, 2… (L+2). In particular, Parks and McClellan found that, for the given set of the extremal frequencies,

$$\delta=\frac{\sum_{k=1}^{L+2} b_k H_d\left(e^{j\omega_k}\right)}{\sum_{k=1}^{L+2} \frac{b_k(-1)^{k+1}}{W(\omega_k)}} \tag{4.23}$$

Where

$$b_k=\prod_{\substack{i=1\\ i\neq k}}^{L+2} \frac{1}{(x_k-x_i)} \tag{4.24}$$

and x_i= $\cos\omega_i$. That is, if $A_e(e^{j\omega})$ is determined by the set of coefficients α_k that satisfy (4-16), Parks and McClellan algorithm used the Lagrange interpolation formula to obtain

$$A_e\left(e^{j\omega}\right)=P(\cos\omega)=\frac{\sum^{L+1}\left[d_k/(x-x_k)\right]C_k}{\sum_{k=1}^{L+1}\left[d_k/(x-x_k)\right]} \tag{4.25}$$

where x = $\cos\omega$, x_i= $\cos\omega_i$

$$C_k=H_d\left(e^{j\omega}\right)-\frac{(-1)^{k+1}\delta}{W(\omega_k)} \tag{4.26}$$

and

$$d_k=\prod_{\substack{i=1\\ i\neq 1}}^{L+1}\frac{1}{(x_k-x_i)}=b_k\left(x_k-x_{L+2}\right) \tag{4.27}$$

[10].

Parks-McClellan algorithm starts with guessing the (L+2) extremal frequencies. After giving a set of frequencies and knowing δ, samples of the amplitude response $A(\omega)$ can be directly calculated from

$$A(\omega_k)=\frac{(-1)^{k(+1)}}{W(\omega_k)}\delta+A_d\left(\omega_k\right) \tag{4.28}$$

The flowchart of Parks-McClellan algorithm is following. In this algorithm, all the impulse response values $h_e[n]$ are absolutely varied on each repeat to obtain the desired optimal approximation.

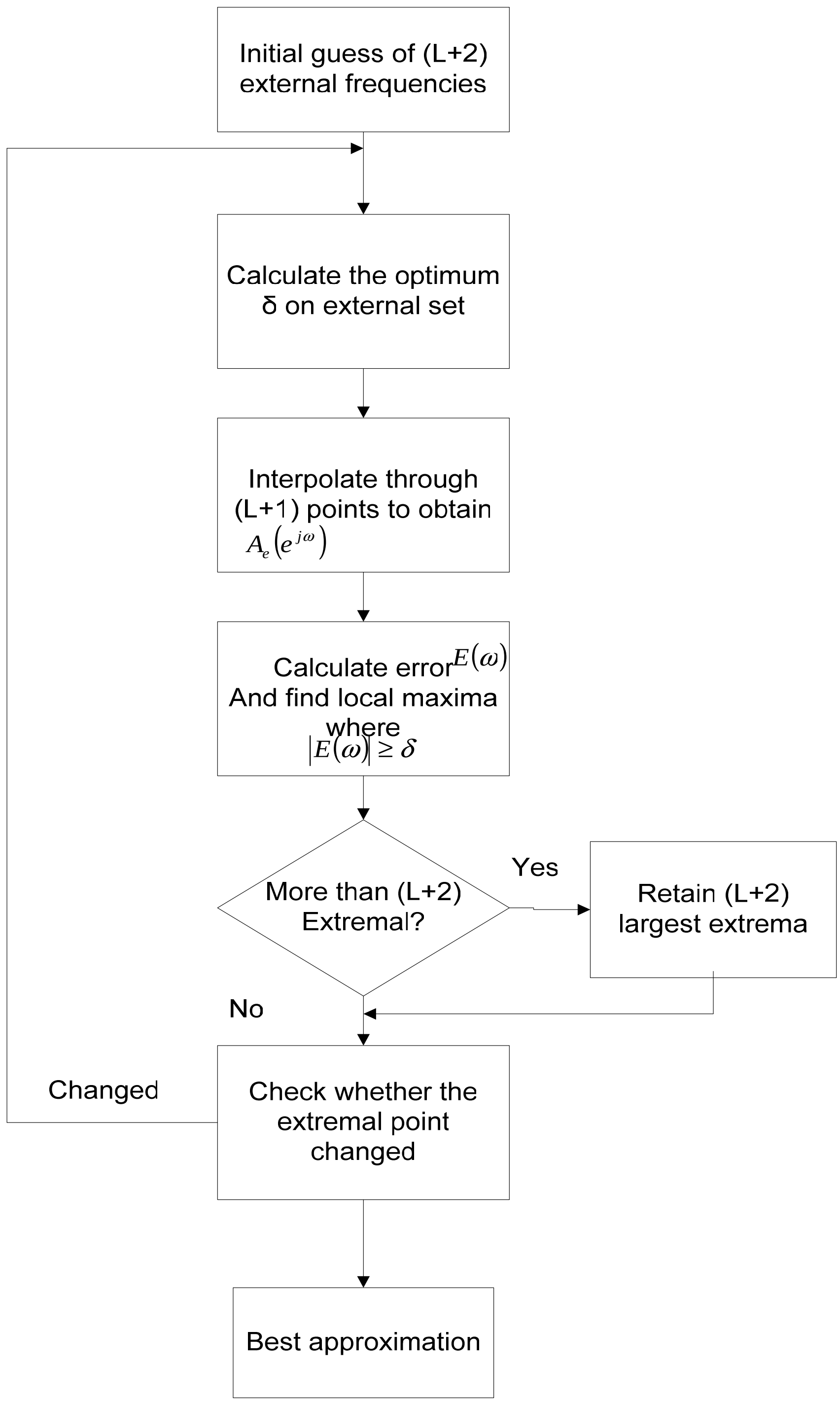

Figure 4.4 Flow chart of Parks-McClellan algorithm [10]

Using the viewpoint of the Remez method, we find that the extremal frequencies are exchanged for a completely new set defined by the (L+2) largest peaks of the error.

4.3.1.2 Remez Exchange Algorithm

The Remez exchange algorithm is a powerful procedure that uses iteration techniques to solve a variety of minimax problems. (A minimax problem is one in which the best solution is the one that minimizes the maximum error that can occur.) Before initiating the process, a set of discrete frequency points is defined for the passband and stopband of the filter. (Transition bands are excluded.) This dense grid of frequencies is used to represent the continuous frequency spectrum.

Extremal frequencies will then be located at particular grid frequencies as determined by the algorithm. The basic steps of the method as it is applied to our filter design problem are shown below.

The procedure of Remez Exchange Algorithm

I. Make an initial guess as to the location of $x + 1$ extremal frequencies, including an extremal at each band edge.

II. Using the extremal frequencies, estimate the actual frequency response by using the Lagrange interpolation formula.

III. Locate the points in the frequency response where maximums occur and determine the error at those points.

IV. Ignore all new extremals beyond the number initially set in I.

To optimize the FIR filter, the Parks-McClellan algorithm first uses the Remez Exchange Algorithm to adjust the frequency to compute h[t] and then optimize $A_e(e^{j\omega})$. At the end of the Remez Exchange Algorithm, the Chebyshev approximation was used to check the criteria $|E(\omega)| \leq \delta$. If $|E(\omega)| > \delta$, the Remez Exchange Algorithm will adjust the frequency until the criteria is met.

The Remez Exchange Algorithm is given by:

$$\begin{bmatrix} H_d(\omega_1) \\ H_d(\omega_2) \\ H_d(\omega_3) \\ \vdots \\ H_d(\omega_K) \end{bmatrix} = \begin{bmatrix} 1, 2\cos(\omega_1), \cdots, 2\cos[\omega_1 L], \dfrac{1}{W(\omega_1)} \\ 1, 2\cos(\omega_2), \cdots, 2\cos[\omega_2 L], \dfrac{1}{W(\omega_2)} \\ \vdots \\ 1, 2\cos(\omega_K), \cdots, 2\cos[\omega_K], \dfrac{1}{W(\omega_K)} \end{bmatrix} \begin{bmatrix} h_0 \\ h_1 \\ h_2 \\ \vdots \\ h_l \\ \delta \end{bmatrix} \tag{4.29}$$

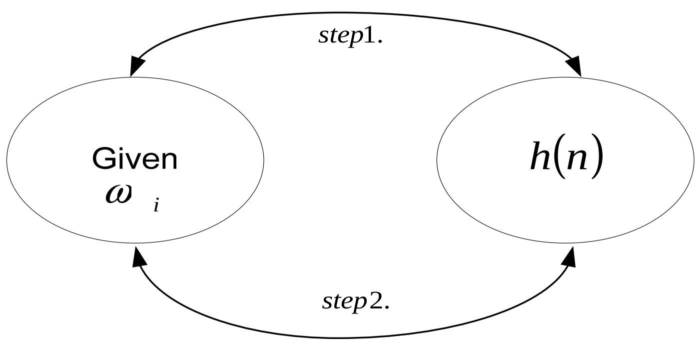

Figure 4.5 Remez exchange algorithm

*step*1.: Given ω_i, find h (n)

*step*2.: Given h (n), find ω_i

This algorithm optimizes the FIR filter design to short the tap number of FIR filter.

4.4 FIR filter Design and Simulation Result in Matlab

4.4.1 FIR Filter Design Rules

For design the FIR filter, first T_d should be constant for all Taps. The output waveform of the FIR filter must meet FCC regulation; the frequency operation range is 3.1GHz ~ 10.6GHz. For implementing the FIR filter, the coefficients a_k, delay time T_d and tap number N should be found.

4.4.2 FIR filter Design

The firpm function was used to produce the impulse response of our FIR filter. Firpm designs a linear-phase FIR filter using Parks-McClellan algorithm. As mentioned before, The Parks-McClellan algorithm uses the Remez exchange algorithm and Chebyshev approximation theory to design filters. They use an optimal fit between the desired and actual frequency responses. The filters are optimal in the sense that the maximum error between the desired frequency response and the actual frequency response is minimized.

The following procedures describe how to design the FIR filter in Matlab.

b = firrpm (n,f,a) proceeds row vector b containing the n+1 coefficients of the order n FIR filter whose frequency response – amplitude characteristics match those given by vectors f and a.

The output filter coefficients (taps) in b obey the symmetry relation:

$$b(k) = b(n+2-k), \qquad k = 1, \ldots, n+1$$

Vectors “f” and “a” specifies the frequency-magnitude characteristics of the filter:

f is a vector of pairs of normalized frequency points, specified in the range between 0 and 1, where 1 corresponds to the Nyquist frequency. The frequencies must be increasing order. Since the FIR filter is for the UWB application, in the actual design, the lower and higher frequency for the bandpass filter is according the UWB regulation: 3.1 GHz~10.6 GHz.

a is a vector containing the desired amplitudes at the points specified in f.

The desired amplitude at frequencies between pairs of points (f(k), f(k+1)) for k odd is the line segment connecting the points (f(k), a(k), and (f(k+1), a(k+1)). The desired amplitude at frequencies between pairs of points for k even is unspecified. The areas between such points are transition or “don’t care” regions. The “don’t care” region will affect the shape of the output pulse.

f and a must be the same length. The length must be an even number.

The follow figure shows the relationship between a, f, and “don’t care region”.

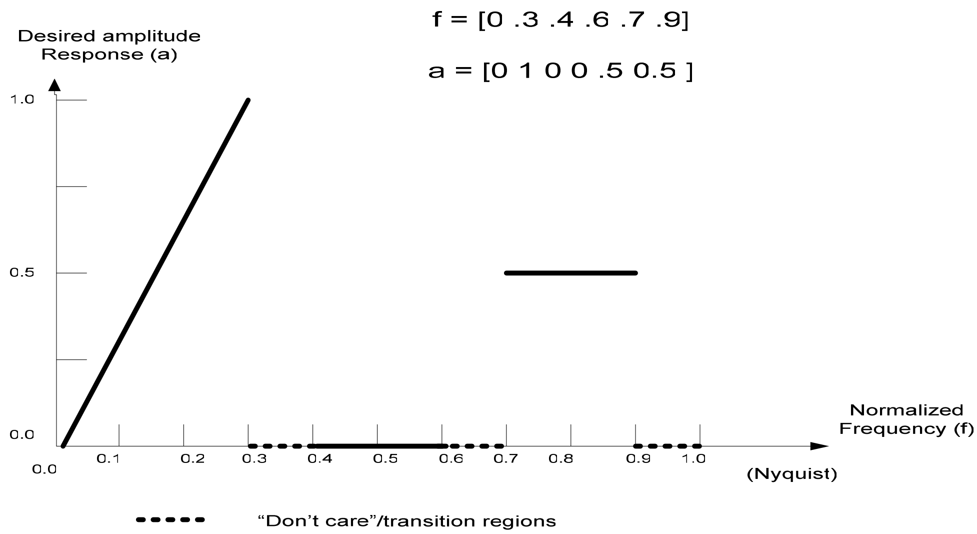

Figure 4.6 The relationship between frequency and desired amplitude response

firmp always uses an even filter order for configurations with a passband at the Nyquist frequency. This is because for odd orders, the frequency response at the Nyquist frequency is necessary 0. If state an odd-valued n, firmpm increments it by 1.

Using firpm to design FIR filter, tap number, frequency vector and amplitude vector should be given. According to FCC regulations, the frequency vector should be between 3.1GHz and 10.6GHz. The desired amplitude vector "a" contains the desired amplitudes at the points specified in the frequencies of the frequencies of the pass band.

Applying the delay time of 30 ps and using 15 taps, firpm generates h[t] Figure 4.7.

Impulse response: h[t] = [0.0123 0.0347 0.0039 -0.1098 -0.1449 0.0578 0.2873 0.1757 -0.1757 -0.2873 -0.0578 0.1449 0.1098 -0.0039 -0.0347 -0.0123]. The 15-tap FIR's phase response is linear phase response as shown in Figure

4.8. A Linear phase response means that all frequencies in the system have the same propagation delay.

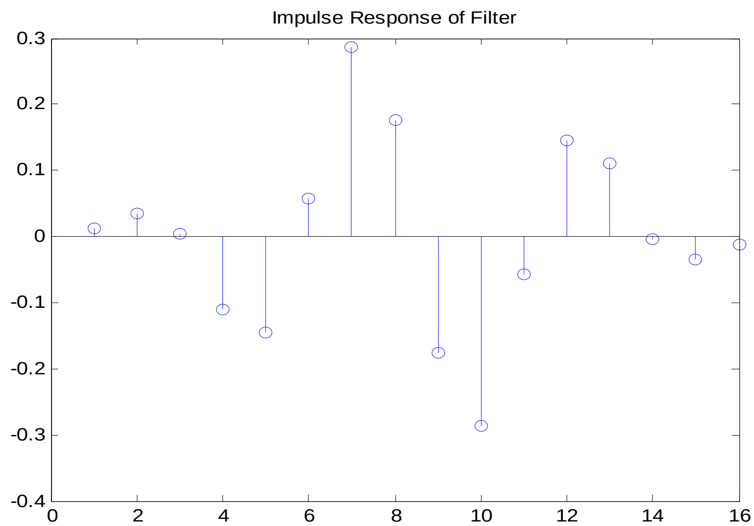

Figure 4.7 Impulse response of FIR filter

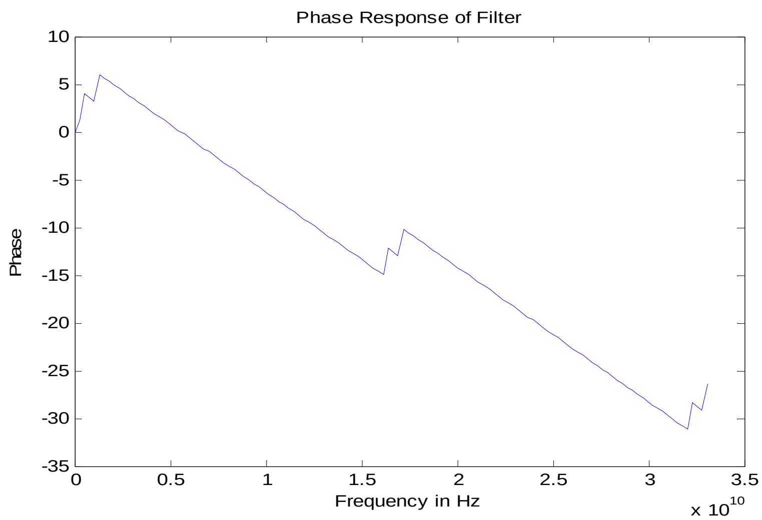

Figure 4.8 Phase response of FIR filter

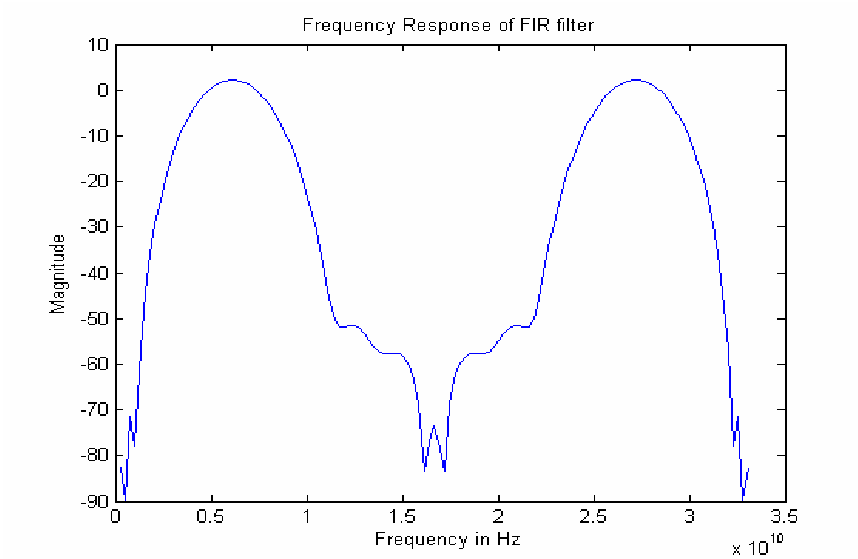

Figure 4.9 Frequency response of FIR filter

4.4.3 Simulation Results

For shaping the Gaussian pulse g[t] coming out from the XOR gate (Figure 4.10), the FIR filter designed from a differentiator convolve the pulse with impulse response h[t] which is shown in Figure 4.7 to generate the 5^{th} derivative Gaussian pulses. The Gaussian pulse from XOR, simulating in ADS, is exported to the Matlab (Figure 4.11). From this output Gaussian, the power spectrum density does not meet the FCC mask as Figure 4.12 showing. The designed FIR filter convolves the exported pulse generate the 5^{th} derivative Gaussian pulse in time domain as in Figure 4.13. Comparing the PSD of before FIR filter and after FIR filter, the 5^{th} derivative Gaussian meet the FCC regulation in Figure 4.14. This is the desired waveform for the Pulsed-UWB wireless system.

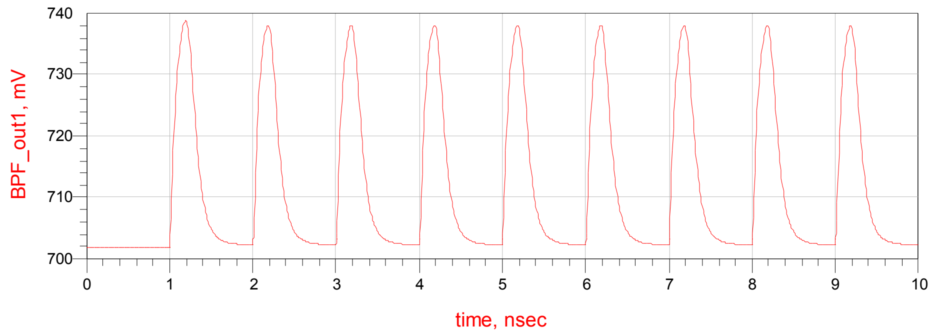

Figure 4.10 1GHz input clock and the last output wave at each cells of a pulse generator

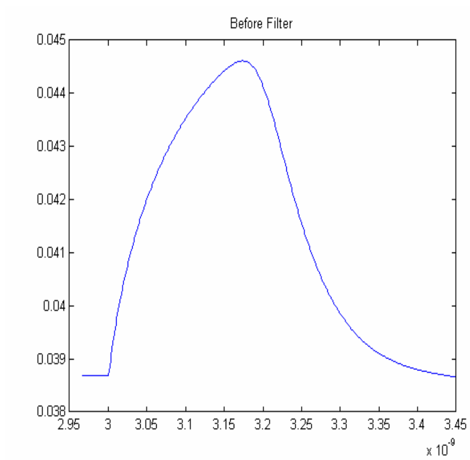

Figure 4.11 The pulse before FIR filter

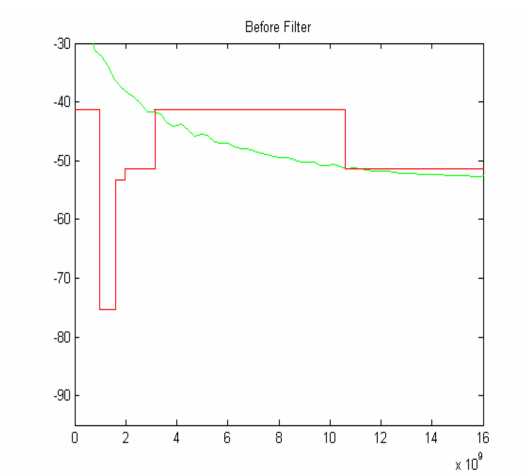

Figure 4.12 The PSD before FIR filter

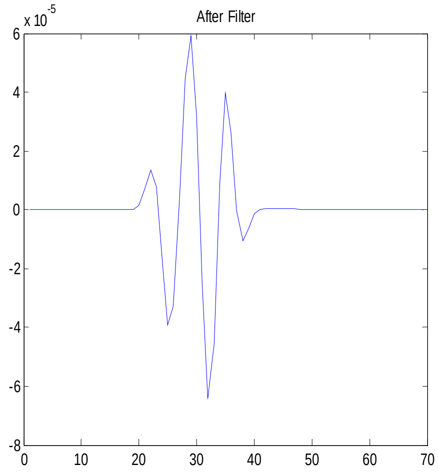

Figure 4.13 The pulse after FIR filter

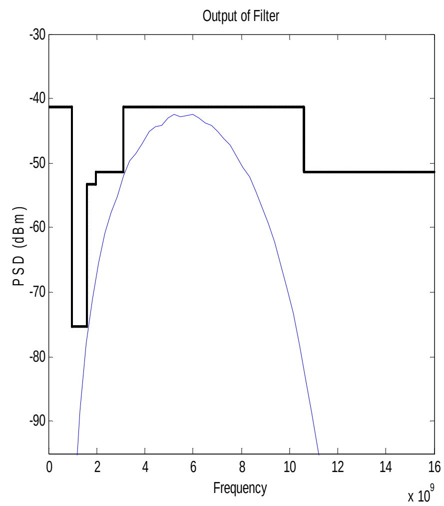

Figure 4.14 The PSD after FIR filter

The continuous-time FIR filter as the pulse shaper generates 5th derivative Gaussian.

$$y[t] = g[t] \otimes h[t]$$

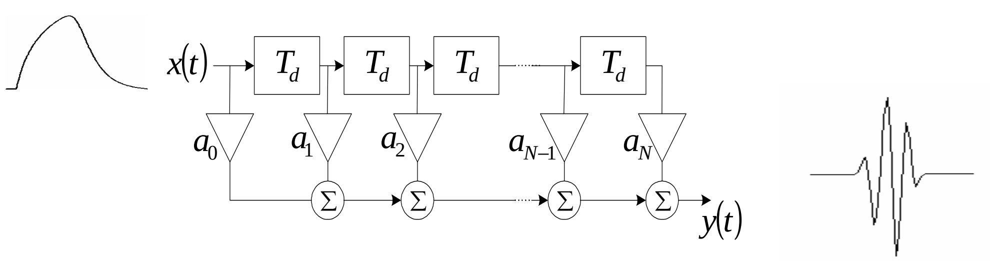

Figure 4.15 The approximate Gaussian pulse through FIR filter and generated the 5^{th} derivative Gaussian

Figure 4.16 shows the response of the impulse generator compared with the ideal 5^{th} order derivative of the Gaussian pulse. When compared with the ideal case in Figure 4.16, it can be seen that an approximate output waveform closely resembling the ideal fifth order derivative of the Gaussian pulse.

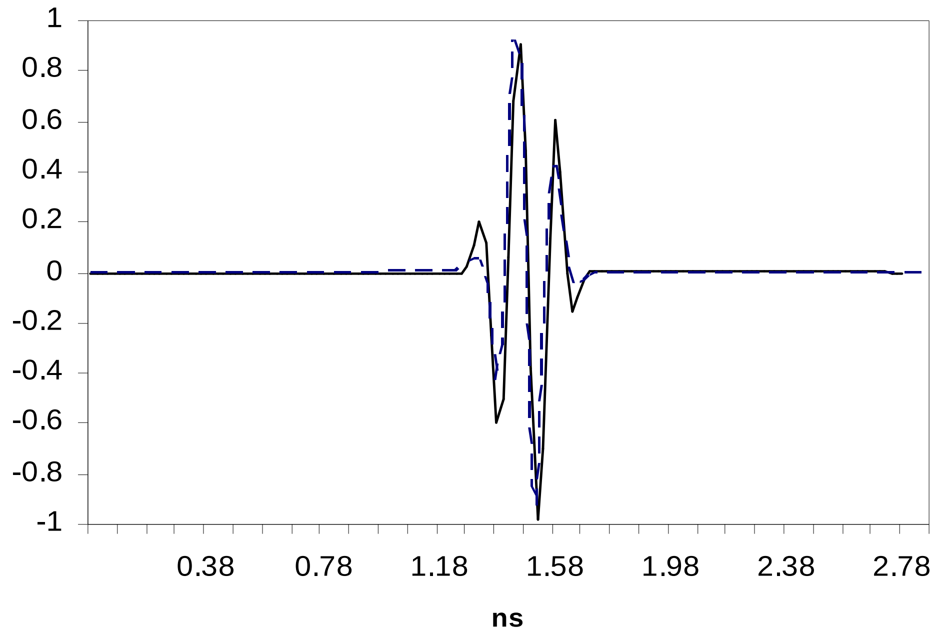

Figure 4.16 The comparison of the ideal 5th derivative Gaussian and the pulse after FIR filter

CHAPTER 5

THE SIMULATION RESULT OF IMPULSE GENERATOR

As mentioned in chapter 3, this impulse generator consists of interpolation delay blocks and an XOR block for the pulse generation, and the pulse shaping FIR filter for impulse shaping. The design and simulations were performed with MATLAB 7.0.4 in conjunction with Advanced Design System (ADS). The circuitry was implemented in the TSMC 0.18μm CMOS process.

When the input signal with frequency 1GHz, V_L=1v, V_H=1.6v is passed through four delay blocks into an XOR gate and compared with the original input signal through an XOR gate, approximate Gaussian pulses are generated. The magnitude of the output pulse is 738mV. The pulse repetition frequency (PRF) is 1 Gb/sec. The pulse width is decided by the delay line. The pulse width has been controlled by the delay time (delay cell) to the target width.

The purpose is making the pulse in the UWB frequency range: 3.1GHz~10.6GHz The generated approximate Gaussian pulses are exported from ADS to MATLAB. The imported pulse g[t] is convoluted with the impulse response h[t] of the FIR filter to generate the 5th derivative Gaussian pulse in the time domain. From the mathematic model for UWB pulses is based on the resemblance of the Gaussian pulse to monopulse and the fact that its *n*th derivative has *n* zero crossings. Comparing the 5th derivative pulse which generated by FIR filter and the ideal 5th derivative Gaussian pulse, there are the same root's numbers: 5 in both figures [15]. To calculate the power spectrum density (PSD) in the frequency domain, the exported pulse should be transferred from time domain to frequency domain. After the pulse shaping, the PSD of the pulse fits within the FCC mask.

CHAPTER 6

CONCLUSION AND FUTURE WORK

For an impulse Radio Ultra-Wide-Bandwidth (UWB) wireless communication system, an all CMOS pulse generator with a 15-tap FIR filter was designed. By adjusting the control voltage, a short duration approximated Gaussian pulse was generated from the XOR gate. The Parks-McClellan algorithm minimizes the maximum error between the desired and actual frequency response to optimize the FIR filter design. In MATLAB, the firpm function using the Parks-McClellan algorithm produces the impulse response of the FIR filter. A 15-tap FIR filter as a differentiator shapes the approximated Gaussian pulse. By convoluting the input signal with the FIR filter's coefficients, the 5^{th} derivative Gaussian pulse has been created. As an IR UWB signal source, the generated pulse should meet FCC regulations. According to the simulation result, the PSD of the pulse coming from the XOR gate can not meet the FCC mask. However, after shaping the pulse using designed FIR filter, the PSD of the pulse is within the FCC regulations.

In generating the 5^{th} derivative pulse, the 15-tap FIR filter plays an important role. Implementing the FIR filter's coefficients and delay block with CMOS transistors is the future work.

REFERENCES

[1] Liuqing Yang; Giannakis, G.B.; "Ultra-Wideband communication: An Ideal Whose Time Has Come" Signal Processing Magazine, IEEE Volume 21, Issue 6, Nov. 2004 Page(s):26 – 54 Digital Object Identifier 10.1109/MSP.2004.1359140.

[2] Bagga, S.; de Vita, G.; Haddad, S.A.P.; Serdijn, W.A.; Long, J.R., "A PPM Gaussian pulse generator for ultra-wideband communications" Circuits and Systems, 2004. ISCAS '04. Proceedings of the 2004 International Symposium on Volume 1, 23-26 May 2004 Page(s):I-109 - I-112 Vol.1.

[3] Welborn, M.; McCorkle, J.; "The Importance of Fractional Bandwidth in Ultra-Wideband Pulse Design", Communications, 2002. ICC 2002. IEEE International Conference on Volume 2, 28 April-2 May 2002 Page(s):753 - 757 vol.2.

[4] Sheng, H, Orlik, P., Haimovich, A.M., Cimini, L.J., and Zhang, J.: "On the spectral and power requirements for ultra-wideband transmission'. IEEE Int. Conf. on Communications, Anchorage, AL, USA, March 2003, Vol. 1, pp. 738–742.

[5] Youngkyun Jeong; Sungyong Jung; Jin Liu; "A CMOS impulse generator for UWB wireless communication systems", Circuits and Systems, 2004. ISCAS '04. Proceedings of the 2004 International Symposium on Volume 4, 23-26 May 2004 Page(s):IV - 129-32 Vol.4.

[6] Chang, Jae J. and Brooke, Marin A.,: "A Clock Extraction Circuit Using Passive Components-Free Filter in Standard Digital Process" IEEE J. of International

[7] Symposium on Circuits and Systems, vol. ISCAS 2000, pp. II-261-264, May 28-31, 2000.

[8] Noboru Ishihara and Y. Akazawa, : “A Monolithic 156Mb/s Clock and Data Recovery PLL Circuit Using the Sample-and-Hold Technique” IEEE J. of Solid-State Circuits, vol. SC-29, pp. 1566-1571, Dec. 1994.

[9] Razavi, Behzad,: “Design of Analog CMOS Integrated Circuits”, McGRAW-HILL International Edition, 2001, 518-520.

[10] Papoulis, Athanasios,: “Circuits and Systems a modern approach”, Holt Rhinehart and Winston, New York, 1980.

[11] **A.** V. Oppenheim and R. W. Schafer. Discrete-Time Signal Processing, Prentice Hall, Englwood Cliffs, New Jersey, 1999.

[11]. Kim, H.; Park, D.; Joo, Y.,”All-Digital Low-Power CMOS Pulse Generator for UWB Systems” Electronics Letters Volume 40, Issue 24, 25 Nov. 2004 Page(s):1534 – 1535.

[12]. Yuanjin Zheng; Han Dong; Yong Ping Xu; “A Novel CMOS/BiCMOS UWB Pulse Generator and Modulator“Microwave Symposium Digest, 2004 IEEE MTT-S International Volume 2, 6-11 June 2004 Page(s):1269 - 1272 Vol.2.

[13]. Saha, P.K.; Sasaki, N.; Kikkawa, T.; “A CMOS UWB transmitter for intra/inter-chip wireless communication” Spread Spectrum Techniques and Applications, 2004 IEEE Eighth International Symposium on 30 Aug.-2 Sept. 2004 Page(s):962 – 966.

[14]. Dongsong Zeng,: “Pulse Shaping Filter Design and Interference Analysis in UWB Communication Systems”, research project for Ph.D., Virginia Polytechnic Institute and State University

[15]. Win, M. Z., Scholtz, R. A., “Ultra-Wide Bandwidth Time-Hopping Spread-Spectrum Impulse Radio for Wireless Multiple-Access Communications” Communications, IEEE Transactions on Volume 48, Issue 4, April 2000 Page(s):679-689.

[16]. Ramachandran, I.; S,; “Acquisition of Direct-Sequence Ultra-Wideband Signals” Wireless Communications and Network Conference, 2005 IEEE Volume 2, 13-17 March 2005 Page(S): 752-757 Vol: 2 Digital Object Identifier 10.1109AWCNC.2005.1424602.

[17]. Maria-Gabriella Di Benedetto, “Understanding Ultra Wide Band Radio Fundamentals”, Prentice Hall.

[18]. Zhao, J.; Maxey, C.; Narayanan, A.; Raman, S.;” A SiGe BiCMOS Ultra Wide Band RFIC Transmitter Design for Wireless Sensor Networks” Radio and Wireless Conference, 2004 IEEE 19-22 Sept. 2004 Page(s):215 – 218.

[19]. Yuanjin Zheng; Han Dong; Yong Ping Xu; “A Novel CMOS/BiCMOS UWB Pulse Generator and Modulator“Microwave Symposium Digest, 2004 IEEE MTT-S International Volume 2, 6-11 June 2004 Page(s):1269 - 1272 Vol.2.

[20]. Stoica, L.; Tiuraniemi, S.; Rabbachin, A.; Oppermann, I. “An Ultra Wideband TAG Circuit Transceiver Architecture“Ultra Wideband Systems, 2004. Joint with Conference on Ultrawideband Systems and Technologies. Joint UWBST & IWUWBS. 2004 International Workshop on 18-21 May 2004 Page(s):258 - 262.

[21]. Authorization of Ultrawideband Technology, First Report and Order, Federal Communications Commission, February 14, 2002.

[22]. M. Alioto and G. Palumbo,: “Modeling and Optimized Design of Current Mode MUX/XOR and D Flip-Flop” IEEE J. of Transactions on Circuits and Systems-II: Analog and Digiral Signal Processing, vol. 47, No. 5, pp. 452-461, May. 2000.

[23]. Jafar Savoj and Behzad Razavi,: “A 10-Gb/s CMOS Clock and Data Recovery Circuit” Symposium on VLSI Circuits Digest of Technical Papers, pp. 136-139, 2000

[24]. Reed, Jeffrey, Buehrer, R. Michael and McKinstry, David,: “Introduction to UWB: Impulse Radio for Radar and Wireless Communications”, Mobile & Portable Radio Research Group, Virginia Polytechnic Institute & State University.

[25]. J. Foerster, E. Green, S. Somayazulu, and D. Leeper, “Ultra-wideband technology for short- or medium-range wireless communications,” *Intel Technology Journal*, pp. 1–11, 2nd Quarter, 2001.

[26] Musicer, Jason,: “An analysis of MOS Current Mode Logic for Low Power and High Performance Digital Logic”, research project for MS, University of California at Berkeley.

BIOGRAPHICAL INFORMATION

Shin-Chih Chang is a candidate for the Master of Science degree at the University of Texas at Arlington. She received her Bachelor of Science degree in Electrical Engineering from the National Cheng-Kung University in Taiwan in 1992. Shin-Chih worked in Philips Electronics Company from 1994 to 2001 as a process engineer. In 2004 spring, she joined the AMIC and is under the supervision of Dr. Sungyong Jung to design and test the UWB transmitter operating blocks for wireless communication systems.